

Learn what you can't learn: Regularized Ensembles for Transductive Out-of-distribution Detection

Alexandru Țifrea, Eric Stavarache, Fanny Yang
 Department of Computer Science
 ETH Zurich, Switzerland
 {tifreaa,ericst,fan.yang}@ethz.ch

December 11, 2020

Abstract

Machine learning models are often used in practice if they achieve good generalization results on in-distribution (ID) holdout data. When employed in the wild, they should also be able to detect samples they cannot predict well. We show that current out-of-distribution (OOD) detection algorithms for neural networks produce unsatisfactory results in a variety of OOD detection scenarios, e.g. when OOD data consists of unseen classes or corrupted measurements. This paper studies how such “hard” OOD scenarios can benefit from adjusting the detection method after observing a batch of the test data. This *transductive* setting is relevant when the advantage of even a slightly delayed OOD detection outweighs the financial cost for additional tuning. We propose a novel method that uses an artificial labeling scheme for the test data and regularization to obtain ensembles of models that produce contradictory predictions only on the OOD samples in a test batch. We show via comprehensive experiments that our approach is indeed able to significantly outperform both inductive and transductive baselines on difficult OOD detection scenarios, such as unseen classes on CIFAR-10/CIFAR-100, severe corruptions (CIFAR-C), and strong covariate shift (ImageNet vs ObjectNet).¹

1 Introduction

Modern machine learning (ML) systems can achieve good test set performance and are gaining popularity in many real-world applications - from aiding medical diagnosis [5] to making recommendations for the justice system [1]. In reality however, some of the data points in a test set can be quite different from the training (in-distribution) data. For example, sampling biases can lead to spurious correlations in the training set [39], a faulty sensor can produce novel data corruptions [29], or new unseen classes can emerge over time, e.g. undiscovered bacteria [38]. Many of these samples are so different compared to the training distribution that a model cannot have enough information to predict their labels. However, it often still outputs predictions with high confidence.

¹Our code is publicly available at <https://github.com/ericpts/reto>

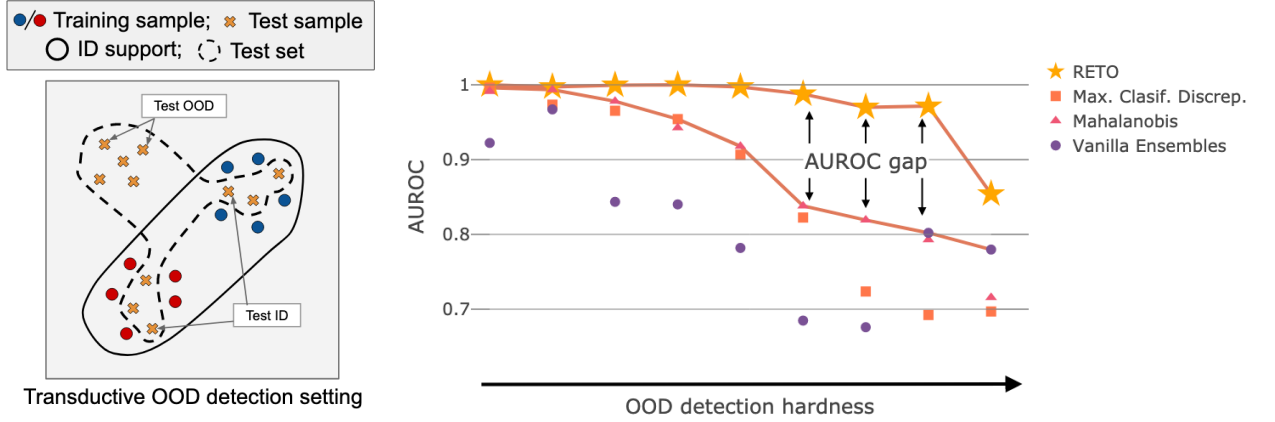


Figure 1. Left: Transductive OOD detection setting. Labeled training set (circles) and an unlabeled test set (crosses) with samples both in- and outside the support of the training distribution. **Right:** Performance of RETO and some baselines on data sets ranked with respect to our method’s AUROC. The solid lines show the gap between RETO and the next best baseline. The gap is wider for hard OOD detection settings.

It is important to identify these out-of-distribution (OOD) samples in the test set and flag them, for example to abstain from prediction [15] and involve a human in the loop.

To achieve this, Bayesian methods [13, 31] or alternatives such as Deep Ensembles [24] try to identify samples on which a given model cannot predict reliably. Their aim is to obtain predictive models that simultaneously have low error on in-distribution (ID) data and perform well in OOD detection. Other approaches try to identify samples with low probability under the training distribution, independent of the prediction model, and use, for instance, density estimation [32] or statistics of the intermediate layers of a neural network [26].

Most prior work have reported good OOD detection performance, almost reaching a perfect area under the ROC curve (AUROC) value of 1. However, these settings generally consider two vastly different data sets such as SVHN vs CIFAR10 as ID and OOD data. We show that the picture is in fact very different in other relevant cases. Specifically, for unseen classes within CIFAR10 or for data with strong distribution shifts (e.g. (resized) ImageNet vs ObjectNet [4]), the AUROC of state-of-the-art methods often drops below 0.85. Figure 1 Right illustrates this drop in performance for some state-of-the-art OOD detection methods for different scenarios.

Almost all of these methods assume a setting where at test time, no training is possible and the OOD detection method can only be trained beforehand. This *inductive setting* allows real-time decision-making and is hence more broadly used. However, in many cases we can indeed predict on batches, for example when sensor readings arrive every second and it is sufficient to make a prediction and decision every few minutes (e.g. automatic irrigation system). In this case we have the entire batch of unlabeled test data available. We can hence use it together with the labeled training set to detect the OOD points in the test batch. We call this the *transductive OOD setting* related to, but quite different from transductive classification [45]. In Section 2.1 we discuss why transductive OOD detection can be very useful even in an online setting.

(How) Can we achieve significantly better OOD detection performance in the transductive setting?

Even though the transductive setting improves test accuracy in small data settings for tasks such as classification or zero-shot learning, it is unclear how to successfully leverage the simultaneous availability of training and test data in the transductive OOD detection setting. A concurrent recent work [49] tackles this challenge by encouraging two neural network classifiers to output different predictions on the test samples (maximum discrepancy). However, this leads to models that disagree to a similar degree on both ID and OOD data so that one cannot distinguish them from one another (see Figure 1). We introduce a new method called Regularized Ensembles for Transductive OOD detection (RETO) for overparameterized models, which heavily uses regularization to make sure that the ensemble disagrees *only on the OOD* samples in the test set, but not on the ID samples. In summary, our main contributions in this paper are as follows:

- We experimentally identify many realistic OOD scenarios where SOTA methods achieve a subpar AUROC below 0.84. We hence argue that the field of OOD detection is far from satisfactorily solved and future methods should include these (or other) hard OOD cases as benchmarks.
- For the transductive OOD detection setting, we propose a new procedure, RETO, that diversifies the output of an ensemble only on the OOD portion of the test set and hence achieves significant improvements compared to SOTA methods (see Figure 1) with a relative gain of at least 32%.²

2 Regularized Ensembles for Transductive OOD detection

In this section we introduce our method for overparametrized classification models, RETO. It exploits the fact that a sufficiently regularized model cannot simultaneously generalize well and fit arbitrary (wrong) labels on ID samples. At the same time, fitting any label on OOD data (away from the majority of the ID points) does not affect generalization, even for regularized models.

2.1 Transductive OOD detection

In an inductive OOD detection setting, one can only tune a method before test time. That is, for any test set, it has to be used with the same fixed parameters. In contrast, in a transductive setting, the training data is available during test time and it is possible to tune a method using both the training set and the specific unlabeled test set. We stress that no labels are available for the test data, so it is unknown which test samples are indeed anomalous. Moreover, we do not assume access to any *known* OOD samples, unlike some of the inductive methods, which sometimes use OOD data for training or calibration [26, 28, 31, 8].

We want to briefly elaborate on the fundamental differences to other transductive settings. When deployed in the context of classification, transductive and semi-supervised learning methods leverage the unlabeled data to obtain low-dimensional representations that are more effective for the prediction task. A key assumption for the setting to be useful is that the data is related in

²We compute the relative gain as $\frac{\mathcal{E}_{\text{RETO}} - \mathcal{E}_{\text{baseline}}}{\mathcal{E}_{\text{baseline}}}$, where $\mathcal{E} := 1 - \text{AUROC}$.

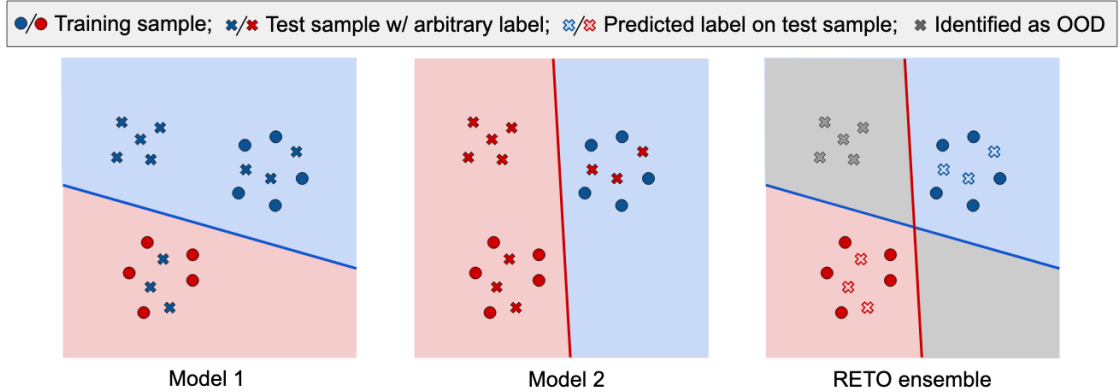


Figure 2. Cartoon illustration of an ensemble of two linear classifiers that fit both the training set and the test set that is assigned the blue label (Model 1) and the red label (Model 2) respectively. Linear classifiers are *smooth enough* that they disagree only on the OOD points in the test set (gray crosses) and agree to predict the correct label on the test ID samples.

some way, e.g. the unlabeled data comes from the same distribution as the labeled data. On the other hand, transductive OOD detection differs from the usual transductive classification setting. The training distribution does not carry information about the OOD data and, as a consequence, it is not obvious how to adapt existing semi-supervised methods to work for transductive OOD detection.

One downside that prevents transductive classification methods from being used more broadly is that for each test set that we want to predict, we would need to have access to the training data and computational resources. Furthermore, these methods do not allow predictions on the fly in the online setting. For transductive OOD detection however, both of these shortcomings can be tolerated. For a prediction task, we can still use the (inductive) classification model to predict test points on the fly, and *only flag OOD samples with a slight delay* after collecting a batch of test points. For example, Covid-19 test results have a crucial role in controlling the spread of the virus. Imagine that a machine learning model is deployed for fast testing and that the model works well under usual circumstances. However, if a test pipeline becomes defective, informing the patient of the potentially wrong test result is crucial, since it may change the quarantine status of that patient. Generally, transductive OOD detection is most useful in situations involving measurement or sensor failures and when the cost of a delayed prediction is justified by the need for accurate predictions.

2.2 The complete RETO procedure

We now provide details on our approach, RETO, outlined in Algorithm 1. We consider the classification problem of learning a map from the input space \mathcal{X} to a discrete set of labels \mathcal{Y} . The (ID) training data is drawn from a distribution P . We consider as OOD any sample outside the support of the training distribution, i.e. $x \in \mathcal{X} \setminus \text{supp}_P$.³

In this paper we focus primarily on settings where we can readily find an overparametrized

³With a slight abuse of notation, we denote by $\text{supp}_P \subset \mathcal{X}$ the support of the marginal distribution P_X .

classification model that generalizes well on in-distribution data. That is, we train models using a combination of optimization algorithm, loss function and hyperparameters that data scientists have found to generalize well on the ID data set. Ultimately, our goal is to construct diverse ensembles of such classification models, that predict different labels on OOD samples.

Recall that we have access to both a labeled training set, and the unlabeled test set. We begin by assigning an arbitrary label (selected from the set of labels of the training data) to all the test samples. We train a classifier on the union of the correctly-labeled training set, and the arbitrarily-labeled test set. To find the optimal classifier, we search among functions that generalize well on the ID (training) distribution. If the classifiers are smooth enough, they cannot fit both the correct labels of the training set and the arbitrary label on the ID test samples, as illustrated in Figure 2 for linear classifiers. However, they can still fit the arbitrary label on the OOD test samples. Through regularization, we ensure that the models we obtain are not too complex. We search inside a hypothesis class of regularized functions, \mathcal{F}_{reg} , as discussed in more detail in Section 3. We ensemble several such classifiers, where each model fits a different label to the test set, while at the same time having good generalization in-distribution, measured on a holdout (ID) validation set. Using a disagreement statistic, we flag as OOD all the points in the test set with high disagreement. To avoid training the ensemble from scratch for each new test batch, it is possible to instead start from pre-trained weights and perform a few iterations of fine-tuning, as detailed in Section 4.

Determining OOD samples with RETO. We distinguish between ID and OOD data using an approach reminiscent of a two-sample statistical test. Consider two finite-sample sets, namely the training set $\{x_i : x_i \sim P_X, 1 \leq i \leq n\}$ ⁴ and the set that only contains one test point $\{x : x \sim Q_X\}$. The null hypothesis is $H_0 : \text{supp}_P = \text{supp}_Q$ and, if it is rejected, it indicates that the test sample x is OOD. Previous baselines have proposed their own choices of the test statistic, which are discussed in detail in Appendix A. For a RETO ensemble of K classifiers, we use:

$$T_{\text{avg-TV}}(x) := \frac{1}{K(K-1)} \sum_{i \neq j} d_{\text{TV}}(f_i(x), f_j(x)),$$

the average pairwise total variation distance between the softmax outputs $f_i(x), f_j(x) \in \mathbb{R}^{|\mathcal{Y}|}$ of models $i, j \in \{1, \dots, K\}$ in the ensemble, where d_{TV} is the total variation distance. The null hypothesis is rejected for high values of $T_{\text{avg-TV}}$. Appendix L contains more details about the choice of the test statistic. It follows from the way in which the hypothesis test is stated that true positives are OOD samples that are indeed flagged as OOD, while the false positives are ID samples that are incorrectly predicted as OOD.

Algorithm 1: Pseudocode for RETO

Input : Train set S , Test set T , Ensemble size K , Test statistic threshold t_0 , Regularized function class \mathcal{F}_{reg} , Disagreement metric

Result: O , i.e. the elements of T which are OOD
Sample K different labels $\{y_1, \dots, y_K\}$ from \mathcal{Y}

for $c \leftarrow \{y_1, \dots, y_K\}$ **do** // train K models

$T^c \leftarrow \{(x, c) : x \in T\}$

$\hat{f}_c \leftarrow \text{Train}(S \cup T^c; \mathcal{F}_{\text{reg}})$

$O = \emptyset$

for $x \in T$ **do** // run two-sample test

if $\text{disagreement}(\hat{f}_{y_1}(x), \dots, \hat{f}_{y_K}(x)) > t_0$ **then**

$O \leftarrow O \cup \{x\}$

return O

⁴We are interested in identifying anomalous covariates, so we discard the labels when performing the statistical test.

3 Why RETO can work well

In this section we provide insights as to why RETO can achieve a higher AUROC for hard OOD settings. Firstly, we elaborate on the rationale behind using ensembles and explain why model diversity is important. We show that a key for RETO to perform well is that the models of the ensemble are “regular” enough. Finally, we argue that early-stopped neural networks represent a hypothesis class that satisfies our conditions.

Ensemble-based OOD detection The main argument for using an ensemble for OOD detection is that a diverse enough set of models will lead to disagreement only on OOD samples. In other words, the models will produce contradictory predictions on OOD inputs, while giving similar predictions for ID data. In order to get a diverse set of models, Deep Ensembles [24] use the stochasticity of the training process. However, the models obtained with this procedure are still very similar and tend to agree on OOD data (Figure 3), especially in hard OOD detection scenarios. In the transductive setting, our method exploits the additional information available in the unlabeled test set to generate ensembles that are more diverse on the OOD test samples. This approach allows the ensembles to work well even when the ID and OOD data are very similar.

We denote the test set as T and consider a partition of it into a test ID set T_{ID} and a test OOD set T_{OOD} . If we were given $T = T_{\text{OOD}}$, we could just enforce different models to predict different labels on T by simply assigning one of the labels $c \in \mathcal{Y}$ to the whole test set, and training model \hat{f}_c in the ensemble on $S \cup T^c$, where $T^c := \{(x_i, c) : x_i \in T\}$. But, obviously, we are given the union of the test ID and test OOD set $T = T_{\text{OOD}} \cup T_{\text{ID}}$, without being able to distinguish between the two.

How can we encourage an ensemble to disagree (only) on T_{OOD} ?

Could we use the same strategy of assigning an arbitrary label to the entire test set? Unfortunately, overparametrized models, such as neural networks, can easily learn random labels [51]. Hence, if we train a neural network to convergence on $S \cup T^c$, *the models will also disagree on the test ID data* (see Figure 3 - Right). How can we enforce models to have contradictory predictions on T_{OOD} but to *agree* on T_{ID} ?

3.1 Key for transductive OOD detection: Regularization

We can remedy this issue with strong regularization of the models in the ensemble. The *key intuition* is that it is difficult to fit an arbitrary label on ID data that is near or between the training samples. The signal in the correctly labeled ID points from the training set prevents an arbitrary label from being easily fit on the ID test samples. This is illustrated in Figure 2, for linear classifiers. Conversely, it is easy to learn the arbitrary label on samples that are far enough from the training data, which are, by definition, the OOD test samples we want to detect! For instance, when training neural networks with SGD, the arbitrary label will be fit much faster on the OOD test samples than on the ID test samples.

What is the right complexity for the models in the ensemble?

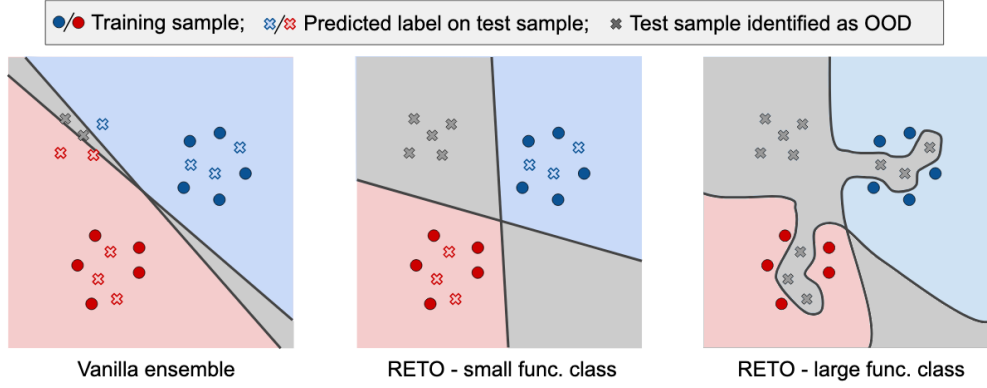


Figure 3. Trade-off between power and false positive rate for different kinds of ensembles used for OOD detection. **Left:** A vanilla ensemble is not diverse enough. **Middle:** RETO classifiers disagree on the OOD points in the test set (gray crosses) and still agree to predict the correct label on the test ID samples. **Right:** The models in the ensemble are too complex so they can easily fit the arbitrary label on the ID test samples as well, thus identifying the whole test set as OOD.

In the language of hypothesis testing, the model complexity should be small enough to limit *false positives* (i.e. ID samples incorrectly flagged as OOD) and large enough to have enough *power* (i.e. identify correctly OOD samples). We encourage high power by making the models fit different labels on the test set, and reduce false positives by *regularizing* the function class just enough. Specifically, we constrain our search to a hypothesis class that is just able to learn the labels on OOD, but not on ID test samples.

Controlling false positives We now describe a necessary condition on the complexity of the model class, required in order to control the false positive rate of RETO. First of all, recall that in our use case we have classifiers available that generalize well in-distribution. This makes sure that the predictive models have enough common ground to agree on the test ID samples.

However there may be model classes which generalize well but are still able to fit arbitrary labels on ID data. Hence, we consider the set of *regularized functions with low population error*, i.e. $\mathcal{F}_\epsilon^\star := \{f \in \mathcal{F}_{\text{reg}} : \mathbb{E} [\mathbb{1}_{f(x) \neq y}] < \epsilon\}$, where \mathcal{F}_{reg} is a restricted function class (e.g. functions parametrized by neural networks regularized via early-stopping). The required amount of regularization is captured in the following condition.

Condition 3.1 ($\mathcal{F}_\epsilon^\star$ has little disagreement in-distribution). *The probability of a point drawn from the ID distribution to be misclassified by a function in $\mathcal{F}_\epsilon^\star$ is at most δ for a small constant $\delta > \epsilon$.*

This condition makes sure that any ensemble of functions from $\mathcal{F}_\epsilon^\star$ disagrees at most on a set of measure δ with respect to the marginal distribution of X . Disagreeing on a point in this set means that there exist at least two functions in $\mathcal{F}_\epsilon^\star$ that predict different outcomes for the same covariates.

From the definition of the class $\mathcal{F}_\epsilon^\star$ it follows that any function in it may misclassify a different subset of \mathcal{X} , of measure at most ϵ . The union of these subsets contains the ID samples on which an ensemble of classifiers from $\mathcal{F}_\epsilon^\star$ can disagree. In the worst case, if K different functions predict wrong labels on pairwise *disjoint* subsets $S_k \subset \mathcal{X}, k \in [K]$, then an ensemble of these functions will

disagree on ID samples with probability $K\epsilon$, which can be high, for large enough K . Condition 3.1 requires that the union of these subsets $\bigcup_{k=1}^K S_k$ have small measure of at most δ , even in the worst case: functions in \mathcal{F}_ϵ^* are smooth enough that they can only predict wrong labels in roughly the same regions of \mathcal{X} (e.g. in the neighborhood of the decision boundary), leading to large overlaps between these subsets. As a consequence, if the condition is satisfied, functions from \mathcal{F}_ϵ^* will “ignore” the wrong labels assigned to the ID test samples, with high probability $1 - \delta$.

Notes on power Note that Condition 3.1 enforces ensemble agreement on ID points to limit the amount of false positives. The power (ensemble disagreement on OOD) depends very much on the support of the OOD samples and its relation to \mathcal{F}_ϵ^* . In Figure 4 we show a test OOD set on which linear classifiers always agree to predict one label. In this case, the boundary between the OOD and ID set requires higher complexity and larger function class is needed (Figure 4 Right). We leave as future work a thorough analysis of the trade-off between the function class size and the detection capabilities of RETO.

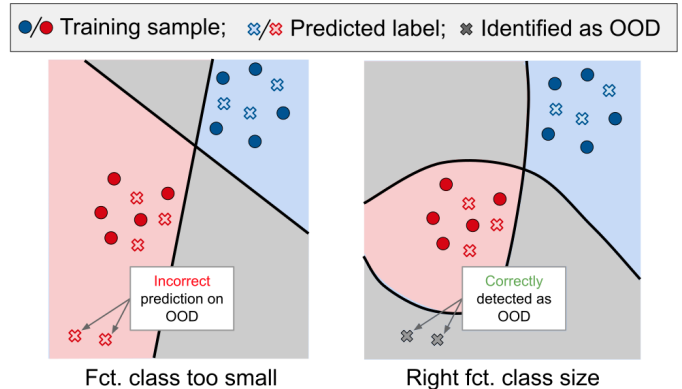


Figure 4. Impact of regularization on power in relation to the OOD support. **Left:** Linear classifiers cannot fit the arbitrary label on test OOD points, and the classifiers will agree on them, leading to low statistical power. **Right:** More complex models can detect this set of test OOD points.

3.2 Regularizing neural networks with early stopping

An example of models that satisfy Condition 3.1 are deep neural networks trained with early stopping. The recent results of [48, 2, 27] suggest that early stopping helps neural networks be more robust to label noise without sacrificing standard accuracy, thus satisfying Condition 3.1. Explicit forms of regularization (e.g. weight decay) may also lead to similar results, but they introduce additional hyperparameters that are difficult to tune.⁵ Figure 5 shows the learning curves obtained when fitting a neural network on S , T_{ID}^c and T_{OOD}^c for a chosen label c : the training set and test OOD samples are fit first and after epoch 50, the predictor starts fitting the wrong label on the test ID set as well. We can also observe that early stopping at the point with the highest accuracy on the validation set (drawn from the same distribution as the training set), captures this phase transition well.

4 Experiments

In this section we evaluate the OOD detection performance of RETO for deep neural networks on several image data sets. We find that our approach outperforms all baselines on difficult OOD detection settings. In addition, we discuss some of the trade-offs that impact our algorithm’s performance.

⁵For each ID and OOD set, we would have to train models to convergence to determine the optimal regularization coefficient that achieves both good statistical power and a low false positive rate.

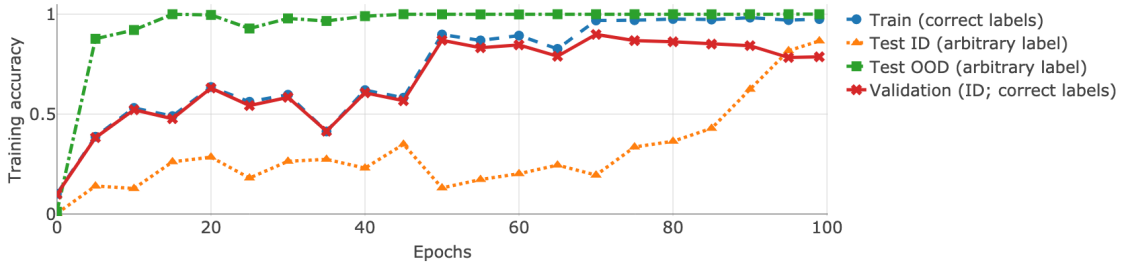


Figure 5. Accuracy measured on the correctly-labeled training set and on the arbitrarily-labeled test ID and OOD subsets, for one model. Validation accuracy is computed on a hold-out set with correctly-labeled ID samples. The training set and the test OOD samples are fit first, while the test ID set reaches high accuracy much later. At epoch 50, the models tend to predict the arbitrary label for test OOD samples and the correct label for test ID. The model is a Resnet20 trained on CIFAR10 as ID and SVHN as OOD.

4.1 ID vs OOD settings

We report results on two broad types of OOD detection scenarios:

1. **Easy OOD data (most previous benchmarks):** ID and OOD samples come from very different data sets (e.g. CIFAR10 vs SVHN). These are the settings usually considered in the OOD detection literature on which most baselines perform well.

2. **Hard OOD data:** We explore two types of more difficult OOD detection tasks (i) The OOD data consists of “novel” classes: e.g. the first 5 digits of SVHN are ID, the last 5 digits are OOD. (ii) The test data suffers from semi-strong covariate shift: e.g. the test set contains corrupted samples from the training distribution (e.g. CIFAR10 vs CIFAR10-C [19]⁶) or samples that violate the spurious correlations present in the training set (e.g. ImageNet vs ObjectNet [4]⁷).

Appendix C provides more insight on OOD detection hardness, while Appendix B presents examples of images for the various settings. Note that we are not too interested in the practical scenario of covariate shift [41], where the distributions are so close that domain adaptation techniques could perform well.⁸ In our hard OOD data sets, domain adaptation also leads to *unsatisfactory results*. For instance, in [43] the authors report a classification error of 20.4% on CIFAR10-C at severity 5, compared to the 8.3% error achieved on the CIFAR10 test set. Alternatively, when domain adaptation fails, OOD detection can prompt a system to abstain on samples from the shifted distribution to prevent erroneous predictions.

Apart from using these canonical data sets, we also compare the performance of our method on more realistic data, namely a recently proposed OOD detection benchmark for medical imaging

⁶Both CIFAR10-C and CIFAR100-C contain 15 types of corruptions, at 5 severity levels. We consider corrupted samples with severity 5.

⁷ObjectNet [4] contains both novel classes that do not appear in ImageNet, and images from ImageNet classes, with strong distribution shift. We resize both ImageNet and ObjectNet to 32x32 images.

⁸These situations when domain adaptation performs well are sometimes more challenging for OOD detection, since it means that ID and OOD data are more similar. In Appendix G.1 we show that RETO maintains its remarkable performance even on the more difficult CIFAR10-C data set with severity 2.

[8]. The authors of this benchmark collected a suite of data sets that cover the aforementioned categories of difficulty, as detailed in Appendix K.

4.2 RETO vs. Baselines

We compare our method against both inductive and transductive baselines. Importantly, some of the baselines require oracle knowledge of some OOD data for training. For example, Outlier Exposure [20] uses TinyImages for training as the set of outliers, irrespective of the OOD set used for evaluation. On the other hand, the *Mahalanobis* baseline [26] is tuned on samples from the same OOD distribution as the one seen at test time. We also present a transductive version of this approach, referred to as *Mahalanobis-T*, on which we elaborate in Appendix A.

For all the baselines, we use the default hyperparameters suggested by their authors on the same ID data set. For RETO, we tune hyperparameters to optimize ID generalization. We defer the details regarding training the models to Appendix A. For evaluation, we use two metrics that are common in the OOD detection literature: the area under the ROC curve (AUROC; larger values are better) and the false positive rate at a true positive rate of 95% (FPR@95; smaller values are better).

4.3 Main results

For our method we train ensembles of five ResNet20 [17] networks (results for other architectures are presented in Appendix G). For each model in the ensemble we perform post-hoc early stopping: we train each model for 100 epochs and select the iteration with the lowest validation loss. For all settings, we used a labeled training set (e.g. 40,000 samples for CIFAR10), a validation set with ID samples (e.g. 10,000 samples for CIFAR10) and an unlabeled test set where half of the samples are ID and the other half are OOD (e.g. 10,000 ID samples and 10,000 OOD samples for CIFAR10 vs SVHN) – see Appendix B for more details.

Table 1 summarizes the main empirical results. We present results for training the models from random initializations (rand init), and for fine-tuning pretrained models (pretrained). Pretraining is always performed on the training set for 100 epochs. When using pretrained weights, as few as three epochs of fine-tuning are enough on average to achieve the performance that we report, which is a significant cut in computation cost. In addition, Appendix D shows the dependence of the OOD detection performance on the ensemble size for RETO and vanilla ensemble.

For the corruption data sets, the table shows the average of the AUROC and FPR@95 taken over all corruptions, and the value for the worst-case setting. Appendix G contains a more detailed breakdown of these numbers.

The evaluation for the scenarios presented in Table 1 is performed on the same test set that was used for training, as usual in transductive learning. In addition to that, the OOD detection performance of RETO extrapolates well to unseen samples from the same distribution (semi-supervised setting).⁹ In order to show this, we run experiments in which we compute the AUROC

⁹This setting is similar for instance to the one in the Mahalanobis baseline, which assumes oracle knowledge of the OOD distribution at training time.

Table 1. We report the AUROC and the FPR@95 of RETO and some baselines for different OOD detection settings (we highlight the **best RETO** variant and **best baseline**). For the corrupted CIFAR data sets, we report the average and the worst-case values over all corruption types. For all settings, the test data is the union of the test splits of the ID and OOD data sets.

ID data	OOD data	kNN	DPN	Vanilla Ensembles Inductive	OE	Mahal.	Mahal-T	MCD	RET (rand init) Transductive	RET (pretrained)
AUROC \uparrow / FPR@95 \downarrow										
SVHN	CIFAR10	0.92 / 0.32	1.00 / 0.00	0.97 / 0.12	1.00 / 0.00	0.99 / 0.02	0.99 / 0.05	0.97 / 0.15	1.00 / 0.01	0.99 / 0.03
CIFAR10	SVHN	0.81 / 0.74	0.95 / 0.15	0.92 / 0.22	0.97 / 0.11	0.99 / 0.04	0.99 / 0.04	1.00 / 0.02	1.00 / 0.00	1.00 / 0.00
CIFAR100	SVHN	0.83 / 0.71	0.77 / 0.56	0.84 / 0.52	0.82 / 0.50	0.98 / 0.10	0.98 / 0.08	0.97 / 0.27	1.00 / 0.00	1.00 / 0.00
SVHN[0:4]	SVHN[5:9]	0.54 / 0.92	0.87 / 0.81	0.92 / 0.31	0.85 / 0.48	0.92 / 0.29	0.91 / 0.37	0.91 / 0.49	0.96 / 0.20	0.94 / 0.34
CIFAR10[0:4]	CIFAR10[5:9]	0.59 / 0.86	0.82 / 0.68	0.80 / 0.61	0.82 / 0.59	0.79 / 0.73	0.64 / 0.87	0.69 / 0.75	0.97 / 0.14	0.91 / 0.34
CIFAR100[0:49]	CIFAR100[50:99]	0.51 / 0.96	0.70 / 0.74	0.78 / 0.65	0.74 / 0.69	0.72 / 0.80	0.72 / 0.81	0.70 / 0.74	0.85 / 0.54	0.81 / 0.60
CIFAR10	CIFAR10-C (avg)	0.67 / 0.72	0.89 / 0.40	0.84 / 0.51	0.86 / 0.46	0.94 / 0.20	0.88 / 0.37	0.95 / 0.16	1.00 / 0.00	1.00 / 0.01
CIFAR10	CIFAR10-C (worst)	0.51 / 0.94	0.72 / 0.90	0.60 / 0.90	0.63 / 0.89	0.78 / 0.73	0.68 / 0.88	0.60 / 0.92	1.00 / 0.00	0.98 / 0.14
CIFAR100	CIFAR100-C (avg)	0.67 / 0.73	0.74 / 0.64	0.78 / 0.63	0.76 / 0.63	0.92 / 0.28	0.84 / 0.45	0.91 / 0.35	1.00 / 0.01	0.99 / 0.03
CIFAR100	CIFAR100-C (worst)	0.51 / 0.94	0.49 / 0.88	0.64 / 0.86	0.62 / 0.87	0.71 / 0.81	0.63 / 0.87	0.60 / 0.90	0.98 / 0.11	0.96 / 0.29
Tiny ImageNet	Tiny ObjectNet	0.51 / 0.96	0.70 / 0.68	0.82 / 0.51	0.79 / 0.63	0.75 / 0.74	0.72 / 0.75	0.99 / 0.02	0.99 / 0.02	0.98 / 0.12
Average		0.67 / 0.77	0.83 / 0.52	0.85 / 0.45	0.85 / 0.46	0.89 / 0.36	0.85 / 0.42	0.90 / 0.33	0.98 / 0.10	0.96 / 0.16

on a hold-out test set drawn from the same ID and OOD data sets as the ones used during training. The AUROC on the hold-out test set is within 0.01 from the one calculated on the test set observed during training.

For the medical OOD detection benchmark we present the average AUROC achieved by some representative baselines in Figure 6a. Our method improves the average AUROC from 0.85 to 0.91, compared to the best performing baseline. We refer the reader to [8] for precise details on the methods. Appendix K contains more results for the medical settings, as well as additional baselines.

Limitations and trade-offs. The results above show that the transductive setting provides enough information to discriminate well between the ID and the OOD test samples, outperforming inductive approaches in many situations. In order to bridge the gap between (offline) transductive OOD detection and online anomaly detection we investigate the impact of the size of the test set on the OOD detection performance. In addition, we also vary the ratio of OOD samples in the test

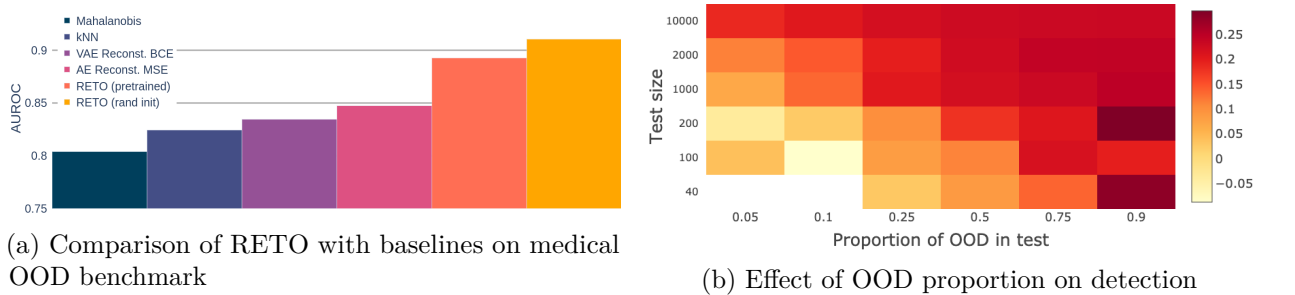


Figure 6. **Left:** AUROC averaged over all scenarios in the medical OOD detection benchmark. The values for the baselines are computed using the code from the paper [8]. **Right:** The gap in AUROC between RETO and a vanilla ensemble, as the number and proportion of ID (CIFAR10) and OOD (CIFAR10-C/snow) samples in the test set is varied. The AUROCs are obtained with an ensemble of ResNet20 models.

set, i.e. $\frac{|T_{\text{OOD}}|}{|T_{\text{ID}}|+|T_{\text{OOD}}|}$. Our findings suggest that there is a broad spectrum of values for which RETO maintains a good performance. In the cases when either the size of the test set or the test OOD ratio is small, the OOD detection performance deteriorates to the point where it is comparable to vanilla ensembles, as shown in Figure 6b where we report the gap in AUROC between RETO and a vanilla ensemble. This loss in efficacy can be mitigated by either splitting the test set in smaller batches, or by using a different labeling scheme for the test set, the details of which we leave as future work.

5 Related work

Transductive learning. Transductive learning [45] has been successfully used for practical applications in problems like zero-shot learning [12, 21, 46]. The transductive setting we consider is also reminiscent of the related problem of unsupervised domain adaptation [6, 14, 23, 10]. Moreover, the paper [40] proposed to solve the transductive anomaly detection problem by discriminating between the training and the test set and constraining the false positive rate using a validation set of ID samples. However, this method does not provide an explicit estimate of the predictive uncertainty of a classifier trained on the labeled training set. In contrast, the RETO ensemble can be used for prediction, and the disagreement statistic is an indication of the ensemble’s confidence.

Ensemble diversity. Previous works have highlighted limitations of ensemble-based OOD detection approaches. Firstly, neural networks tend to make overconfident predictions even on test samples far from the training distribution [18]. Moreover, the stochasticity of conventional neural network training approaches (e.g. random initialization, SGD) is not sufficient to obtain ensembles that are diverse enough to give good uncertainty estimates on OOD samples [30]. Some recent works address this problem by adding explicit regularizers that incentivize model diversity, either in a transductive setting, like MCD [49], or inductively [3]. However they do not manage to detect OOD samples well in hard scenarios.

Bayesian prediction. One of the important appeals of the Bayesian framework is that it directly provides uncertainty estimates together with the predictions, in the form of a posterior distribution. Approaches like MC-Dropout [13] or Deep Prior Networks [31] have been proposed in the context of OOD detection, but the uncertainty estimates they provide are often inaccurate on OOD samples [35]. The same problem has been observed for Bayesian Neural Networks (BNNs) [33, 16, 7]. Moreover, in the case of BNNs, sampling efficiently from the posterior over parameters remains challenging for large models [35].

6 Conclusions

Reliable OOD detection is essential in order for classification systems to be deployed in safety-critical environments. We present a method that achieves state-of-the-art performance in a transductive OOD detection setting, and which, like other approaches, can ultimately be used to abstain on OOD samples. As future work, we propose a more thorough investigation of the influence of the labeling scheme of the test set on the sample complexity of the method, as well as an analysis of the trade-off governed by the complexity of the model class of the classifiers.

Acknowledgments

We are grateful to Călin Cruceru, Gideon Dresdner, Alexander Immer, Sidak Pal Singh and Armeen Taeb for feedback on the manuscript and to Ayush Garg for preliminary experiments. We also thank the anonymous reviewers for their helpful remarks.

References

- [1] J. Angwin, J. Larson, S. Mattu, and L. Kirchner. Machine bias: There’s software used across the country to predict future criminals. and it’s biased against blacks. 2016.
- [2] S. Arora, S. Du, W. Hu, Z. Li, and R. Wang. Fine-grained analysis of optimization and generalization for overparameterized two-layer neural networks. volume 97 of *Proceedings of Machine Learning Research*, pages 322–332, 2019.
- [3] H. Bahng, S. Chun, S. Yun, J. Choo, and S. J. Oh. Learning de-biased representations with biased representations. In *Proceedings of the 37th International Conference on Machine Learning*, 2020.
- [4] A. Barbu, D. Mayo, J. Alverio, W. Luo, C. Wang, D. Gutfreund, J. Tenenbaum, and B. Katz. ObjectNet: A large-scale bias-controlled dataset for pushing the limits of object recognition models. In *Advances in Neural Information Processing Systems 32*, pages 9453–9463. 2019.
- [5] E. Beede, E. Baylor, F. Hersch, A. Iurchenko, L. Wilcox, P. Ruamviboonsuk, and L. M. Vardoulakis. A human-centered evaluation of a deep learning system deployed in clinics for the detection of diabetic retinopathy. In *Proceedings of the CHI Conference on Human Factors in Computing Systems*, page 1–12, 2020.
- [6] S. Ben-David, J. Blitzer, K. Crammer, and F. Pereira. Analysis of representations for domain adaptation. In *Advances in Neural Information Processing Systems 19*, pages 137–144, 2007.
- [7] C. Blundell, J. Cornebise, K. Kavukcuoglu, and D. Wierstra. Weight uncertainty in neural networks. In *Proceedings of the 32th International Conference on Machine Learning*, 2015.
- [8] T. Cao, C.-W. Huang, D. Y.-T. Hui, and J. P. Cohen. A benchmark of medical out of distribution detection. *arXiv preprint arXiv:2007.04250*, 2020.
- [9] B. Chen, W. Liu, Z. Yu, J. Kautz, A. Shrivastava, A. Garg, and A. Anandkumar. Angular visual hardness. *arXiv preprint arXiv:1912.02279*, 2019.
- [10] Y. Chen, C. Wei, A. Kumar, and T. Ma. Self-training avoids using spurious features under domain shift. *arXiv preprint arXiv:2006.10032*, 2020.
- [11] J. Deng, W. Dong, R. Socher, L.-J. Li, K. Li, and L. Fei-Fei. ImageNet: A large-scale hierarchical image database. In *Proceedings of the IEEE Conference on Computer Vision and Pattern Recognition (CVPR)*, 2009.
- [12] Y. Fu, T. M. Hospedales, T. Xiang, and S. Gong. Transductive multi-view zero-shot learning. *IEEE Transactions on Pattern Analysis and Machine Intelligence*, 37:2332–2345, 2015.

- [13] Y. Gal and Z. Ghahramani. Dropout as a Bayesian approximation: Representing model uncertainty in deep learning. volume 48 of *Proceedings of Machine Learning Research*, pages 1050–1059, 2016.
- [14] Y. Ganin, E. Ustinova, H. Ajakan, P. Germain, H. Larochelle, F. Laviolette, M. March, and V. Lempitsky. Domain-adversarial training of neural networks. *Journal of Machine Learning Research*, pages 1–35, 2016.
- [15] Y. Geifman and R. El-Yaniv. Selective classification for deep neural networks. In *Advances in Neural Information Processing Systems 30*, pages 4878–4887. 2017.
- [16] A. Graves. Practical variational inference for neural networks. In *Advances in Neural Information Processing Systems 24*, pages 2348–2356. 2011.
- [17] K. He, X. Zhang, S. Ren, and J. Sun. Deep residual learning for image recognition. In *Proceedings of the IEEE Conference on Computer Vision and Pattern Recognition (CVPR)*, 2016.
- [18] M. Hein, M. Andriushchenko, and J. Bitterwolf. Why ReLU networks yield high-confidence predictions far away from the training data and how to mitigate the problem. In *Proceedings of the IEEE Conference on Computer Vision and Pattern Recognition (CVPR)*, 2019.
- [19] D. Hendrycks and T. Dietterich. Benchmarking neural network robustness to common corruptions and perturbations. In *Proceedings of the International Conference on Learning Representations*, 2019.
- [20] D. Hendrycks, M. Mazeika, and T. Dietterich. Deep anomaly detection with outlier exposure. In *Proceedings of the International Conference on Learning Representations*, 2019.
- [21] E. Kodirov, T. Xiang, Z. Fu, and S. Gong. Unsupervised domain adaptation for zero-shot learning. In *Proceedings of the IEEE/CVF International Conference on Computer Vision (ICCV)*, pages 2452–2460, 2015.
- [22] A. Krizhevsky. Learning multiple layers of features from tiny images. Technical report, 2009.
- [23] A. Kumar, T. Ma, and P. Liang. Understanding self-training for gradual domain adaptation. *arXiv preprint arXiv:2002.11361*, 2020.
- [24] B. Lakshminarayanan, A. Pritzel, and C. Blundell. Simple and scalable predictive uncertainty estimation using deep ensembles. In I. Guyon, U. V. Luxburg, S. Bengio, H. Wallach, R. Fergus, S. Vishwanathan, and R. Garnett, editors, *Advances in Neural Information Processing Systems 30*, pages 6402–6413. Curran Associates, Inc., 2017.
- [25] Y. Lecun, L. Bottou, Y. Bengio, and P. Haffner. Gradient-based learning applied to document recognition. In *Proceedings of the IEEE*, pages 2278–2324, 1998.
- [26] K. Lee, K. Lee, H. Lee, and J. Shin. A simple unified framework for detecting out-of-distribution samples and adversarial attacks. In *Advances in Neural Information Processing Systems 31*, pages 7167–7177. 2018.

- [27] M. Li, M. Soltanolkotabi, and S. Oymak. Gradient descent with early stopping is provably robust to label noise for overparameterized neural networks. *Proceedings of Machine Learning Research*, pages 4313–4324, 2020.
- [28] S. Liang, Y. Li, and R. Srikant. Enhancing the reliability of out-of-distribution image detection in neural networks. In *Proceedings of the International Conference on Learning Representations*, 2018.
- [29] A. X. Lu, A. X. Lu, W. Schormann, D. W. Andrews, and A. M. Moses. The cells out of sample (COOS) dataset and benchmarks for measuring out-of-sample generalization of image classifiers. *arXiv preprint arXiv:1906.07282*, 2019.
- [30] H. Maennel and A. Țifrea. Fourier networks for uncertainty estimates and out-of-distribution detection. 2020.
- [31] A. Malinin and M. Gales. Predictive uncertainty estimation via prior networks. In *Advances in Neural Information Processing Systems 32*, page 7047–7058, 2018.
- [32] E. Nalisnick, A. Matsukawa, Y. W. Teh, D. Gorur, and B. Lakshminarayanan. Do deep generative models know what they don’t know? In *Proceedings of the International Conference on Learning Representations*, 2019.
- [33] R. M. Neal. *Bayesian Learning for Neural Networks*. Springer-Verlag, 1996.
- [34] Y. Netzer, T. Wang, A. Coates, A. Bissacco, B. Wu, and A. Y. Ng. Reading digits in natural images with unsupervised feature learning. In *NIPS Workshop on Deep Learning and Unsupervised Feature Learning 2011*, 2011.
- [35] Y. Ovadia, E. Fertig, J. Ren, Z. Nado, D. Sculley, S. Nowozin, J. Dillon, B. Lakshminarayanan, and J. Snoek. Can you trust your model’s uncertainty? Evaluating predictive uncertainty under dataset shift. In *Advances in Neural Information Processing Systems 32*, pages 13991–14002. 2019.
- [36] B. Recht, R. Roelofs, L. Schmidt, and V. Shankar. Do cifar-10 classifiers generalize to cifar-10? *arXiv preprint arXiv:1806.00451*, 2018.
- [37] B. Recht, R. Roelofs, L. Schmidt, and V. Shankar. Do ImageNet classifiers generalize to ImageNet? *arXiv preprint arXiv:1902.10811*, 2019.
- [38] J. Ren, P. J. Liu, E. Fertig, J. Snoek, R. Poplin, M. Depristo, J. Dillon, and B. Lakshminarayanan. Likelihood ratios for out-of-distribution detection. In *Advances in Neural Information Processing Systems 32*, pages 14707–14718. 2019.
- [39] S. Sagawa, P. W. Koh, T. B. Hashimoto, and P. Liang. Distributionally robust neural networks. In *Proceedings of the International Conference on Learning Representations*, 2020.
- [40] C. Scott and G. Blanchard. Transductive anomaly detection. Technical report, 2008.
- [41] H. Shimodaira. Improving predictive inference under covariate shift by weighting the log-likelihood function. *Journal of Statistical Planning and Inference*, 90:227–244, 2000.

- [42] R. Shwartz-Ziv and N. Tishby. Opening the black box of deep neural networks via information. *arXiv preprint arXiv:1703.00810*, 2017.
- [43] Y. Sun, X. Wang, L. Zhuang, J. Miller, M. Hardt, and A. A. Efros. Test-time training with self-supervision for generalization under distribution shifts. In *Proceedings of the 37th International Conference on Machine Learning*, 2020.
- [44] A. Torralba, R. Fergus, and W. T. Freeman. 80 million tiny images: A large data set for nonparametric object and scene recognition. *IEEE Transactions on Pattern Analysis and Machine Intelligence*, pages 1958–1970, 2008.
- [45] V. N. Vapnik. *Statistical Learning Theory*. Wiley-Interscience, 1998.
- [46] Z. Wan, D. Chen, Y. Li, X. Yan, J. Zhang, Y. Yu, and J. Liao. Transductive zero-shot learning with visual structure constraint. In *Advances in Neural Information Processing Systems 32*, pages 9972–9982, 2019.
- [47] H. Xiao, K. Rasul, and R. Vollgraf. Fashion-MNIST: A novel image dataset for benchmarking machine learning algorithms, 2017.
- [48] F. F. Yilmaz and R. Heckel. Image recognition from raw labels collected without annotators. *arXiv preprint arXiv:1910.09055*, 2019.
- [49] Q. Yu and K. Aizawa. Unsupervised out-of-distribution detection by maximum classifier discrepancy. In *Proceedings of the IEEE/CVF International Conference on Computer Vision (ICCV)*, 2019.
- [50] S. Zagoruyko and N. Komodakis. Wide residual networks. In *Proceedings of the British Machine Vision Conference (BMVC)*, 2016.
- [51] C. Zhang, S. Bengio, M. Hardt, B. Recht, and O. Vinyals. Understanding deep learning requires rethinking generalization. *arXiv preprint arXiv:1611.03530*, 2016.

A Experiment details

A.1 Baselines

We instantiate all baselines with the hyperparameters suggested by the authors for the respective settings (e.g. different hyperparameters for CIFAR10 or ImageNet). For all methods, we use pre-trained models provided by the authors when available and we pre-train our own models when that is not the case. When doing our own pre-training, we always use the parameters described in the original paper. The code published for the *Mahalanobis* method performs a hyperparameter search automatically for each of the settings on which we ran it.

- **k-Nearest Neighbors:** We take $k = 8$. For each test sample, we take the average distance to the nearest neighbors in the input (pixel) space, and we use this as the test statistic.
- **Vanilla Ensembles** [24]: We train an ensemble on the training set according to the true labels. For a test sample, average the models’ probabilities, and use the entropy of the resulting distribution as the test statistic. We use ensembles of 5 models, with the same architecture and hyperparameters as the ones used for RETO.
- **Outlier Exposure** [20]: It makes the model’s softmax predictions close to the uniform distribution on the known outliers, while maintaining a good classification performance on the training distribution. We use the WideResNet(WRN) [50] for the RGB data sets. For fine-tuning, we use their recommended settings of 10 epochs at learning rate 0.001. For training from scratch, we train for 100 epochs with an initial learning rate of 0.1. When the training dataset is either CIFAR and ImageNet, we use the default WRN parameters of the author’s code, namely 40 layers, 2 widen-factor, droprate 0.3. For when the training dataset is SVHN, we use the author’s recommended parameters of 16 layers, 4 widen-factor and droprate 0.4. All settings use the cosine annealing learning rate scheduler provided with the author’s code, without any modifications.
- **Deep Prior Networks (DPN)** [31]: Bayesian Method that trains a neural network (Prior Network) to parametrize a Dirichlet distribution over the class probabilities. We train an WRN-28-10 for 100 epochs using SGD with momentum 0.9, with an initial learning rate of 0.01, which is decayed by 0.2 at epochs 50, 70, and 90. For MNIST, we use EMINST/Letters as OOD for tuning. For all other settings, we use TinyImages as OOD for tuning.
- **Mahalanobis** [26]: It pretrains models on the training data. For a data point, it uses the intermediate representations of each layer as “extracted features”. It then performs binary classification using logistic regression using these extracted features. In the original setting, the classification is done on “training” ID vs “training” OOD samples (which are from the same distribution as the test OOD samples). Furthermore, hyperparameter tuning for the optimal amount of noise is performed on validation ID and OOD data. We use the WRN-28-10 architecture, pretrained for 200 epochs. The initial learning rate is 0.1, which is decayed at epochs 60, 120, and 160 by 0.2. We use SGD with momentum 0.9, and the standard weight decay of $5 \cdot 10^{-4}$.

- **Mahalanobis-Transductive:** The methodology proposed by [26] is very different from the other settings, where we do not have access to samples which are known to be OOD and from the same distribution as test OOD. Therefore, we propose a transductive alternative: early-stopped logistic regression is used to distinguish between the training set and the test set (instead of ID vs OOD samples). The early stopping iteration is chosen to minimize the classification errors on a validation set that contains only ID data (recall that we do not assume to know which are the OOD samples).
- **Maximum Classifier Discrepancy (MCD)** [49]: It is a transductive method that trains two classifiers at the same time, and makes them disagree on the test data, while maintaining good classification performance. We use the WRN-28-10 architecture as suggested in the paper. We did not change the default parameters which came with the author’s code, so weight decay is 10^{-4} , and the optimizer is SGD with momentum 0.9. When available (for CIFAR10 and CIFAR100), we use the pretrained models provided by the authors. For the other training datasets, we use their methodology to generate pretrained models: We train a WRN-28-10 for 200 epochs. The learning rate started at 0.1 and dropped by a factor of 10 at 50% and 75% of the training progress, respectively.

A.2 Training configuration for regularized ensembles

For RETO we use hyperparameters that give the best test accuracy when training a model on the ID training set. We do not perform further hyperparameter tuning for the different OOD data sets on which we evaluate our approach.

For MNIST, we train a 3-layer MLP with ReLU activations. Each intermediate layer has 100 neurons. The model is optimized using Adam, with a learning rate of 0.001, for 10 epochs.

For CIFAR and ImageNet, we train a ResNet20 [17] The model is trained using SGD with momentum 0.9, and the learning rate starts at 0.1, and is multiplied by 0.2 at epochs 50, 70 and 90. The weights have a l2 regularization coefficient of $5e - 4$. We use a batch size of 128 for all scenarios, unless explicitly stated otherwise. The hyperparameters have been selected to achieve high accuracy on the CIFAR100 classification problem, thus obtaining an ensemble validation accuracy of 80.8%, where each individual model has between 77% and 78% accuracy. After that, we used the same hyperparameters for all settings. For the fine tuning scenarios, we trained for 10 epochs with a constant learning rate of 0.001 for all scenarios.

For the medical data sets, we train a Densenet-121 as the authors do in the original paper. For training from scratch, we do not use random weight initializations, but instead we start with the ImageNet weights provided with Tensorflow. The training configuration is exactly the same as for ResNet20, except that we use a batch size of 32 because of GPU memory restrictions, and for fine tuning we use a constant learning rate of 10^{-5} .

B ID and OOD data sets

B.1 Data sets

For evaluation, we use the following image data sets:

- MNIST [25] and Fashion MNIST [47].
- SVHN [34].
- CIFAR10, CIFAR100 [22], and their corrupted variants [19].
- ImageNet [11] and ObjectNet [4], both resized to 32x32.

For the experiments using MNIST and FashionMNIST the training set size is 50,000, the validation size is 10,000, and the test ID and test OOD sizes are both 10,000.

For SVHN, CIFAR10 and CIFAR100, the training set size is 40,000, the validation size is 10,000, and the test ID and test OOD sizes are 10,000.

For ImageNet vs ObjectNet, the training set size is 281,167, the validation size is 1,000,000, the test ID size is 50,000, and the test OOD size is 50,273.

For all of the splits, all the sizes are divided by 2 (since both splits have the same size).

B.2 Samples for the settings with novel classes

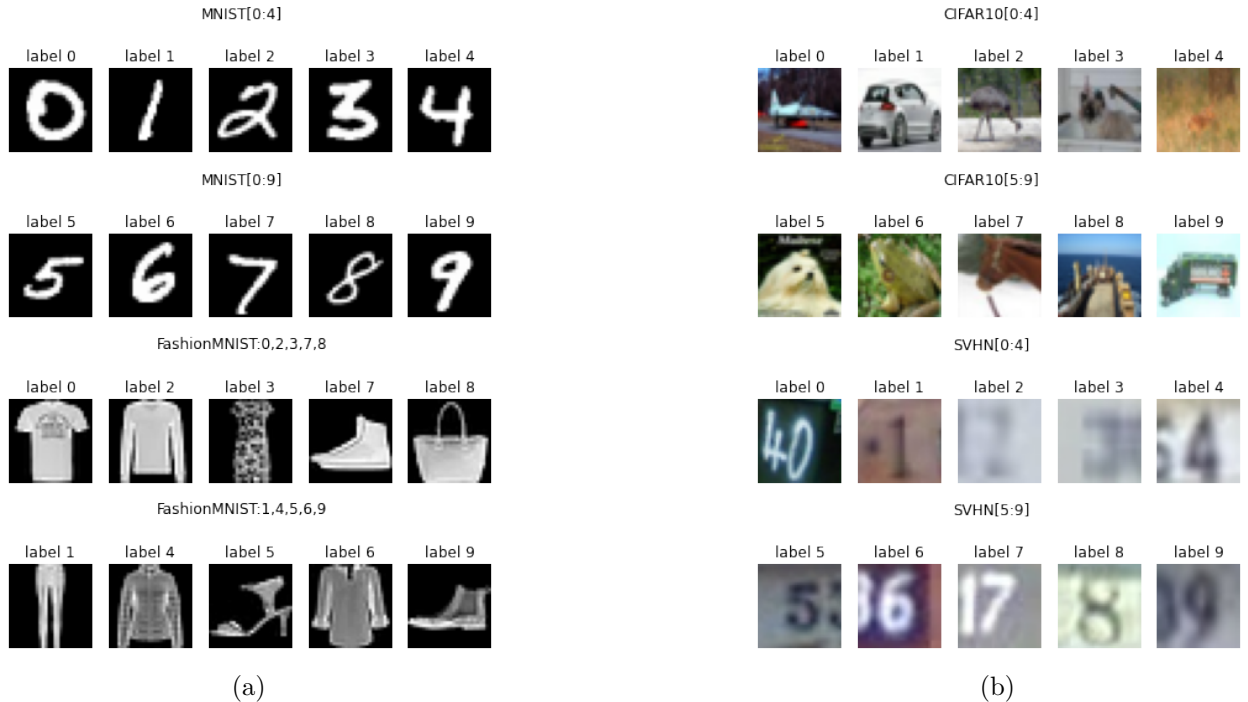


Figure 7. (a) Data samples for the MNIST/FashionMNIST splits. (b) Data samples for the CIFAR10/SVHN splits.

B.3 Samples from ObjectNet

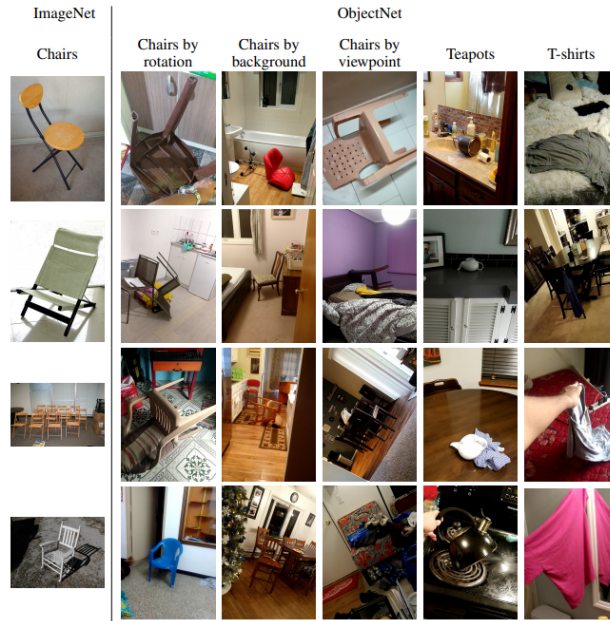


Figure 8: Samples from ImageNet and ObjectNet taken from the original paper by [4].

B.4 Samples from CIFAR10-C

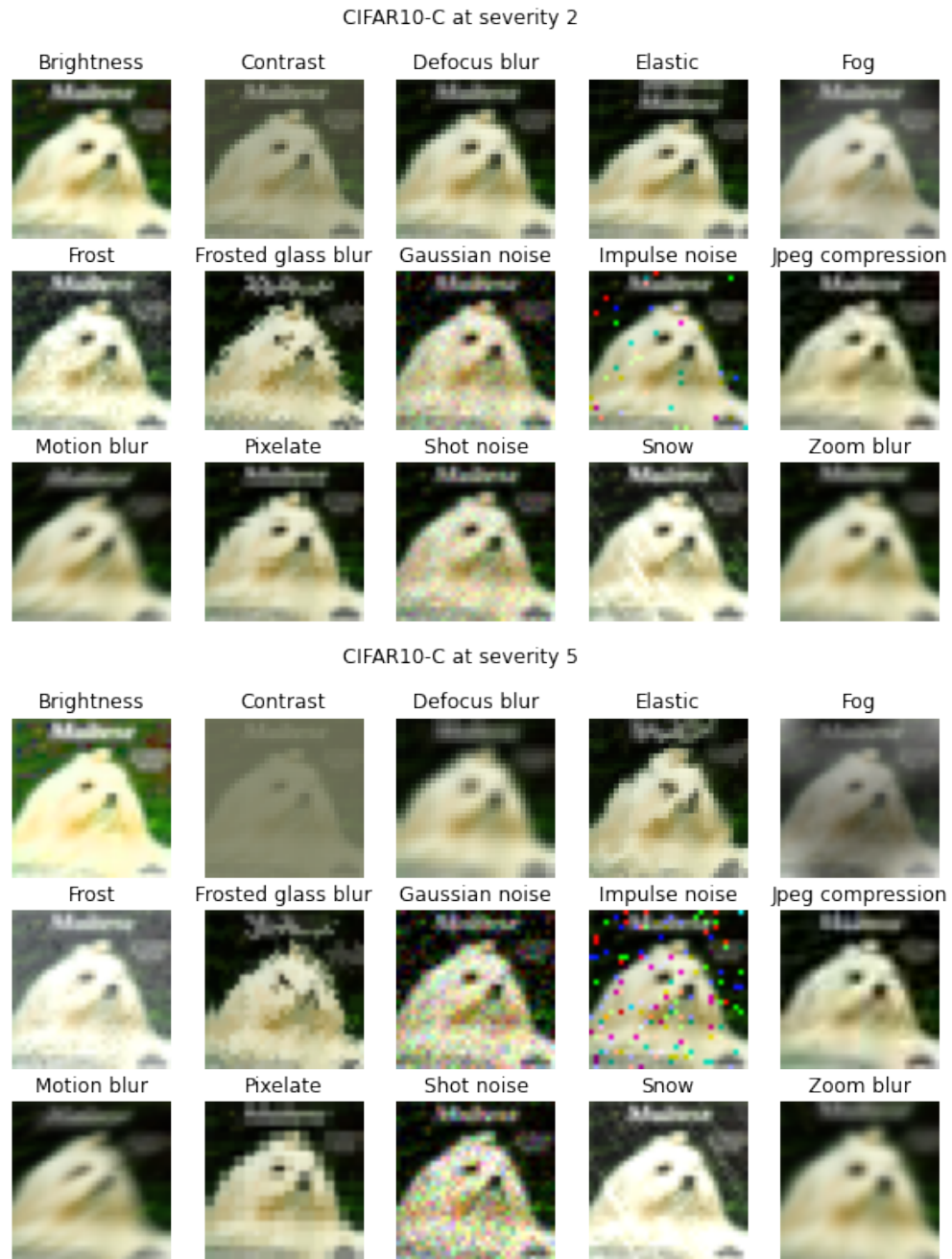


Figure 9: Data samples for the corrupted CIFAR10-C data set.

C OOD detection hardness

Out of distribution detection benchmarks can be assessed based on their difficulty. In what follows, we propose a simple way to evaluate the hardness of an OOD detection setting and provide empirical evidence that shows that the scenarios we looked at are indeed more complicated than some of the common OOD detection benchmarks.

Consider the task of distinguishing between samples that come from two distributions P, Q with disjoint supports $\text{supp}_P, \text{supp}_Q$. Let us assign labels according to the distribution the points are coming from: $\mathcal{D} = \{(x_i, y_i) : y_i = -1 \text{ if } x_i \in \text{supp}_P, y_i = 1 \text{ if } x_i \in \text{supp}_Q\}$. We solve the classification problem by searching for a minimizer of the empirical risk inside a function class \mathcal{F} .

The intuition for our measure of *hardness* is as follows: if it is difficult for a binary classifier to separate samples from P and Q , then it will also be difficult to detect test samples from Q as OOD, when only a training set drawn from P is available.

To quantify the difficulty of the binary classification problem, we use the area under the training curve, i.e. the curve of the training loss as a function of iterations of the optimization algorithm. The larger the area, the more iterations it takes to converge, which in turn indicates that the classification problem is difficult.

Formally, we define the *hardness* of the OOD detection task with respect to a function class \mathcal{F} as:

$$\mathcal{H}_{OODD}(\mathcal{D}; \mathcal{F}) := \int_0^1 L_n(f_t) dt,$$

where f_t is the model after a fraction t of the training epochs are finished and L_n is the empirical loss function.

For our task, we start with a VGG model and train it for 30 epochs. In order to approximate the integral, we take the training loss for the whole data set every 5 epochs, and we average these losses.

Notice that the settings with novel classes and the one with hard covariate shift are generally more difficult than the common benchmarks used in the OOD detection literature.

Apart from the three categories of settings that we introduced in Section 4, we also present numbers for CIFAR10-C and CIFAR100-C with lower-severity corruptions, i.e. severity 2. These scenarios are usually easier to solve with domain adaptation techniques. Nevertheless, in Appendix G we show that RETO performs well on OOD detection on these settings as well. Even though performing OOD detection is redundant here, the good results of our method go to show that it can still work well, even in difficult situations.

Table 2: OOD detection hardness.

	ID data set	OOD data set	\mathcal{H}_{OODD}
1) Easy OOD	MNIST	FashionMNIST	0.01
	FashionMNIST	MNIST	0.01
	SVHN	CIFAR10	0.05
	CIFAR10	SVHN	0.05
	CIFAR100	SVHN	0.06
2) Novel classes	MNIST[0:4]	MNIST[5:9]	0.15
	FashionMNIST:0,2,3,7,8	FashionMNIST:1,4,5,6,9	0.27
	SVHN[0:4]	SVHN[5:9]	0.24
	CIFAR10[0:4]	CIFAR10[5:9]	0.45
	CIFAR100[0:49]	CIFAR100[50:99]	0.59
3) Hard covariate shift	CIFAR10	CIFAR10-C sev5	0.08
	CIFAR100	CIFAR100-C sev5	0.10
	ImageNet	ObjectNet	0.18
3') Easy covariate shift	CIFAR10	CIFAR10-C sev2	0.18
	CIFAR100	CIFAR100-C sev2	0.19

D Resource requirements for RETO

Computational cost Our method can work with training each model in the ensemble from scratch (i.e. random initialization), but it also preforms well when fine-tuning a network from pretrained weights. This reduces significantly the inference time for each batch of test data. For the settings we considered, on average, as few as three epochs of fine tuning are enough to achieve the best performance: the training is stopped early, on average, after three epochs, according to the condition on the validation loss.

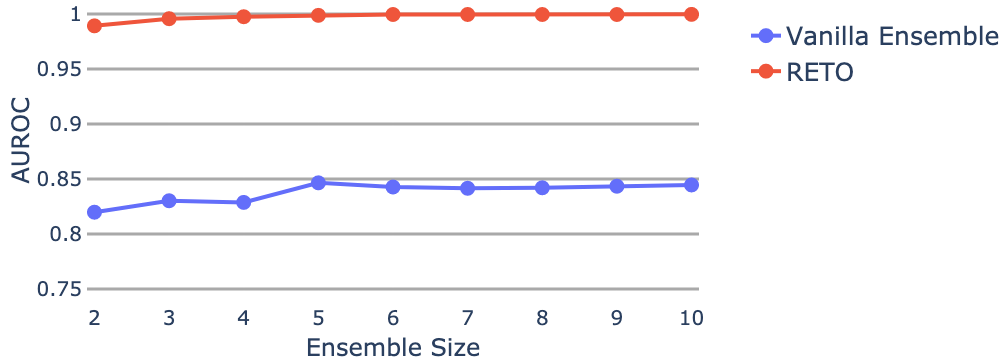


Figure 10. Effect of ensemble size on CIFAR100 vs. SVHN. Both methods are trained from scratch for 100 epochs.

Dependence on ensemble size Figure 10 shows that the good performance of RETO does not rely on a large number of models in the ensemble. Unlike vanilla ensembles, our method achieves a high AUROC with as few as 2 models. This is because, in vanilla ensembles, the networks are diverse ‘by chance’, due to the stochasticity of the training procedure. On the other hand, in RETO, our training method actively encourages the ensembles to be diverse, and hence two models will already disagree on OOD data almost as much as five.

E Generalization to hold-out test set

In this section we present experiments which show that after training/fine-tuning on a test set with ID and OOD samples, one can also use our method to detect OOD samples from the same distribution, that have not been seen during training. Concretely, we use a test set of 5000 ID and 5000 OOD samples to train RETO ensembles (we reiterate that we do not have access to which samples are indeed OOD in the test set). For evaluation, we compute the metrics on a separate data set, with 5000 ID and 5000 OOD samples, where the OOD samples come from the same distribution as the samples seen during training. As revealed in Table 3, the performance does not change substantially, when evaluating on the hold-out test set. For the corruption data sets, we report for each metric the average taken over all corruptions (A), and the value for the worst-case setting (W).

Table 3: Generalization on held out test set.

ID data	OOD data	RETO (normal) AUROC \uparrow / FPR@95 \downarrow	RETO (holdout) AUROC \uparrow / FPR@95 \downarrow
SVHN	CIFAR10	0.99 / 0.03	0.99 / 0.02
CIFAR10	SVHN	1.00 / 0.00	1.00 / 0.00
CIFAR100	SVHN	1.00 / 0.00	1.00 / 0.00
SVHN[0:4]	SVHN[5:9]	0.94 / 0.34	0.95 / 0.28
CIFAR10[0:4]	CIFAR10[5:9]	0.91 / 0.34	0.90 / 0.37
CIFAR100[0:49]	CIFAR100[50:99]	0.81 / 0.60	0.79 / 0.63
CIFAR10	CIFAR10-C sev 2 (A)	0.96 / 0.14	0.95 / 0.16
CIFAR10	CIFAR10-C sev 2 (W)	0.68 / 0.81	0.65 / 0.84
CIFAR10	CIFAR10-C sev 5 (A)	1.00 / 0.01	1.00 / 0.02
CIFAR10	CIFAR10-C sev 5 (W)	0.98 / 0.14	0.97 / 0.21
CIFAR100	CIFAR100-C sev 2 (A)	0.94 / 0.24	0.95 / 0.23
CIFAR100	CIFAR100-C sev 2 (W)	0.71 / 0.81	0.71 / 0.84
CIFAR100	CIFAR100-C sev 5 (A)	0.99 / 0.03	0.99 / 0.03
CIFAR100	CIFAR100-C sev 5 (W)	0.96 / 0.29	0.95 / 0.30
Average		0.97 / 0.11	0.97 / 0.11

F Regularized training/test discriminator for transductive OOD detection

The paper [40] suggests that training a binary classifier with bounded false positive rate to distinguish between the training set S and the test set T can successfully separate the OOD samples from the ID samples in the test set. However, this approach does not fall in the category of predictive uncertainty-based OOD detection methods, since it does not provide a good classifier of the labeled training set as well.

We present in what follows a set of experiments run to check if a similar technique works for the data sets we considered. Early stopping with respect to a validation set that contains only ID samples is enough to obtain good OOD detection performance.

For the corruption data sets, the table shows the average of the AUROC taken over all corruptions (A), and the value for the worst-case setting (W).

Table 4. AUROC for an early-stopped binary classifier trained to separate the training set from the test set.

ID data	OOD data	Binary classifier AUROC \uparrow
SVHN	CIFAR10	0.99
CIFAR10	SVHN	1.00
CIFAR100	SVHN	1.00
SVHN[0:4]	SVHN[5:9]	0.82
CIFAR10[0:4]	CIFAR10[5:9]	0.83
CIFAR100[0:49]	CIFAR100[50:99]	0.61
CIFAR10	CIFAR10-C sev 2 (A)	0.94
CIFAR10	CIFAR10-C sev 2 (W)	0.51
CIFAR10	CIFAR10-C sev 5 (A)	1.00
CIFAR10	CIFAR10-C sev 5 (W)	1.00
CIFAR100	CIFAR100-C sev 2 (A)	0.83
CIFAR100	CIFAR100-C sev 2 (W)	0.50
CIFAR100	CIFAR100-C sev 5 (A)	1.00
CIFAR100	CIFAR100-C sev 5 (W)	1.00
Tiny ImageNet	Tiny ObjectNet	1.00
Average		0.94

G More experiments

G.1 Extended results with ResNet

Table 5. Extended results on all setting (including a breakdown for all corruption types). For RETO and vanilla ensembles, we train 5 ResNet20 models for each setting.

ID data	OOD data	kNN	DPN	Vanilla Ensembles	OE	Mahal.	Mahal-T	MCD	RETO (rand init)	RETO (pretrained)
AUROC \uparrow / FPR@95 \downarrow										
SVHN	CIFAR10	0.92	0.32	1.00	0.00	0.97	0.12	1.00	0.00	0.99 / 0.03
CIFAR10	SVHN	0.81	0.74	0.95	0.15	0.92	0.22	0.97	0.11	0.99 / 0.04
CIFAR100	SVHN	0.83	0.71	0.77	0.56	0.84	0.52	0.82	0.50	0.98 / 0.10
SVHN[0:4]	SVHN[5:9]	0.54	0.92	0.87	0.81	0.92	0.31	0.85	0.48	0.92 / 0.29
CIFAR10[0:4]	CIFAR10[5:9]	0.59	0.86	0.82	0.68	0.80	0.61	0.82	0.59	0.79 / 0.73
CIFAR100[0:49]	CIFAR100[50:99]	0.51	0.96	0.70	0.74	0.78	0.65	0.74	0.69	0.72 / 0.80
CIFAR10	CIFAR10-C brightness 2	0.54	0.93	0.55	0.93	0.51	0.95	0.52	0.94	0.58 / 0.92
CIFAR10	CIFAR10-C contrast 2	0.94	0.20	0.69	0.86	0.59	0.91	0.62	0.89	0.82 / 0.56
CIFAR10	CIFAR10-C defocus blur 2	0.56	0.91	0.48	0.95	0.54	0.93	0.56	0.93	0.67 / 0.81
CIFAR10	CIFAR10-C elastic 2	0.56	0.92	0.47	0.97	0.63	0.87	0.65	0.87	0.71 / 0.76
CIFAR10	CIFAR10-C fog 2	0.81	0.52	0.61	0.89	0.53	0.93	0.55	0.93	0.81 / 0.62
CIFAR10	CIFAR10-C frost 2	0.50	0.92	0.84	0.60	0.69	0.84	0.69	0.85	0.90 / 0.42
CIFAR10	CIFAR10-C frosted glass blur 2	0.51	0.95	0.98	0.09	0.89	0.42	0.86	0.50	0.99 / 0.02
CIFAR10	CIFAR10-C gaussian noise 2	0.57	0.89	0.97	0.13	0.83	0.62	0.85	0.58	1.00 / 0.01
CIFAR10	CIFAR10-C impulse noise 2	0.61	0.85	0.95	0.23	0.80	0.68	0.81	0.61	1.00 / 0.02
CIFAR10	CIFAR10-C jpeg compression 2	0.51	0.95	0.65	0.92	0.71	0.81	0.73	0.77	0.75 / 0.74
CIFAR10	CIFAR10-C motion blur 2	0.60	0.88	0.65	0.88	0.71	0.81	0.74	0.77	0.80 / 0.69
CIFAR10	CIFAR10-C pixelate 2	0.52	0.94	0.82	0.67	0.65	0.88	0.66	0.85	0.79 / 0.71
CIFAR10	CIFAR10-C shot noise 2	0.53	0.92	0.87	0.61	0.74	0.79	0.75	0.82	0.98 / 0.06
CIFAR10	CIFAR10-C snow 2	0.57	0.90	0.85	0.61	0.74	0.76	0.74	0.80	0.96 / 0.18
CIFAR10	CIFAR10-C zoom blur 2	0.59	0.89	0.56	0.96	0.71	0.77	0.73	0.81	0.83 / 0.56
CIFAR10	CIFAR10-C brightness 5	0.56	0.88	0.77	0.78	0.60	0.90	0.63	0.89	0.78 / 0.73
CIFAR10	CIFAR10-C contrast 5	1.00	0.00	0.98	0.08	0.92	0.25	0.96	0.14	1.00 / 0.01
CIFAR10	CIFAR10-C defocus blur 5	0.65	0.82	0.82	0.71	0.88	0.39	0.92	0.25	0.96 / 0.18
CIFAR10	CIFAR10-C elastic 5	0.59	0.89	0.82	0.66	0.80	0.64	0.78	0.74	0.84 / 0.61
CIFAR10	CIFAR10-C fog 5	0.89	0.27	0.93	0.32	0.79	0.69	0.80	0.69	0.98 / 0.10
CIFAR10	CIFAR10-C frost 5	0.70	0.68	0.94	0.27	0.84	0.59	0.84	0.60	0.98 / 0.07
CIFAR10	CIFAR10-C frosted glass blur 5	0.55	0.92	0.97	0.11	0.90	0.37	0.89	0.39	0.99 / 0.05
CIFAR10	CIFAR10-C gaussian noise 5	0.67	0.75	1.00	0.01	0.91	0.30	0.96	0.17	1.00 / 0.00
CIFAR10	CIFAR10-C impulse noise 5	0.83	0.50	0.99	0.04	0.94	0.17	0.98	0.09	1.00 / 0.00
CIFAR10	CIFAR10-C jpeg compression 5	0.51	0.94	0.73	0.87	0.79	0.68	0.81	0.63	0.82 / 0.61
CIFAR10	CIFAR10-C motion blur 5	0.66	0.82	0.81	0.71	0.84	0.59	0.86	0.50	0.91 / 0.27
CIFAR10	CIFAR10-C pixelate 5	0.56	0.92	0.98	0.07	0.84	0.59	0.88	0.49	0.98 / 0.04
CIFAR10	CIFAR10-C shot noise 5	0.66	0.77	0.99	0.01	0.91	0.30	0.95	0.20	1.00 / 0.00
CIFAR10	CIFAR10-C snow 5	0.61	0.84	0.91	0.41	0.77	0.70	0.79	0.72	0.95 / 0.25
CIFAR10	CIFAR10-C zoom blur 5	0.63	0.84	0.72	0.90	0.87	0.48	0.88	0.43	0.96 / 0.12
CIFAR100	CIFAR100-C brightness 2	0.53	0.94	0.54	0.93	0.52	0.94	0.52	0.94	0.55 / 0.93
CIFAR100	CIFAR100-C contrast 2	0.94	0.21	0.62	0.87	0.60	0.90	0.58	0.90	0.75 / 0.71
CIFAR100	CIFAR100-C defocus blur 2	0.56	0.92	0.44	0.96	0.55	0.92	0.54	0.93	0.70 / 0.82
CIFAR100	CIFAR100-C elastic 2	0.55	0.93	0.32	0.97	0.61	0.88	0.59	0.89	0.68 / 0.86
CIFAR100	CIFAR100-C fog 2	0.82	0.52	0.59	0.90	0.55	0.93	0.53	0.93	0.75 / 0.72
CIFAR100	CIFAR100-C frost 2	0.53	0.90	0.73	0.76	0.71	0.79	0.65	0.83	0.82 / 0.65
CIFAR100	CIFAR100-C frosted glass blur 2	0.50	0.95	0.78	0.66	0.79	0.61	0.72	0.72	0.98 / 0.04
CIFAR100	CIFAR100-C gaussian noise 2	0.56	0.89	0.74	0.68	0.81	0.59	0.79	0.56	0.99 / 0.03
CIFAR100	CIFAR100-C impulse noise 2	0.61	0.85	0.83	0.59	0.82	0.59	0.83	0.55	0.99 / 0.03
CIFAR100	CIFAR100-C jpeg compression 2	0.51	0.94	0.63	0.86	0.70	0.79	0.69	0.79	0.71 / 0.82
CIFAR100	CIFAR100-C motion blur 2	0.60	0.89	0.49	0.92	0.68	0.82	0.63	0.85	0.82 / 0.57
CIFAR100	CIFAR100-C pixelate 2	0.52	0.94	0.76	0.75	0.63	0.88	0.61	0.87	0.87 / 0.49
CIFAR100	CIFAR100-C shot noise 2	0.53	0.92	0.70	0.77	0.75	0.73	0.73	0.72	0.94 / 0.23
CIFAR100	CIFAR100-C snow 2	0.55	0.91	0.76	0.73	0.73	0.77	0.69	0.80	0.93 / 0.36
CIFAR100	CIFAR100-C zoom blur 2	0.59	0.90	0.41	0.94	0.69	0.81	0.63	0.85	0.83 / 0.46
CIFAR100	CIFAR100-C brightness 5	0.53	0.93	0.70	0.83	0.64	0.86	0.62	0.87	0.74 / 0.76
CIFAR100	CIFAR100-C contrast 5	1.00	0.01	0.79	0.55	0.78	0.57	0.82	0.53	0.99 / 0.03
CIFAR100	CIFAR100-C defocus blur 5	0.65	0.84	0.54	0.83	0.81	0.63	0.75	0.67	0.96 / 0.15
CIFAR100	CIFAR100-C elastic 5	0.59	0.90	0.73	0.78	0.72	0.76	0.69	0.79	0.71 / 0.81
CIFAR100	CIFAR100-C frost 5	0.90	0.25	0.80	0.60	0.75	0.70	0.70	0.73	0.92 / 0.40
CIFAR100	CIFAR100-C frosted glass blur 5	0.73	0.68	0.78	0.63	0.79	0.63	0.72	0.71	0.94 / 0.26
CIFAR100	CIFAR100-C gaussian noise 5	0.55	0.93	0.80	0.54	0.80	0.60	0.73	0.72	0.97 / 0.08
CIFAR100	CIFAR100-C impulse noise 5	0.67	0.77	0.81	0.54	0.84	0.42	0.85	0.41	1.00 / 0.00
CIFAR100	CIFAR100-C jpeg compression 5	0.84	0.48	0.88	0.37	0.86	0.42	0.96	0.20	1.00 / 0.00
CIFAR100	CIFAR100-C motion blur 5	0.51	0.94	0.69	0.79	0.77	0.71	0.75	0.69	0.82 / 0.61
CIFAR100	CIFAR100-C pixelate 5	0.66	0.83	0.56	0.86	0.76	0.70	0.71	0.74	0.91 / 0.29
CIFAR100	CIFAR100-C shot noise 5	0.55	0.92	0.95	0.17	0.80	0.59	0.80	0.58	0.99 / 0.01
CIFAR100	CIFAR100-C snow 5	0.66	0.79	0.84	0.50	0.83	0.47	0.84	0.44	1.00 / 0.01
CIFAR100	CIFAR100-C zoom blur 5	0.56	0.90	0.80	0.63	0.77	0.70	0.73	0.73	0.90 / 0.45
CIFAR100	CIFAR100-C zoom blur 5	0.64	0.85	0.49	0.88	0.79	0.66	0.74	0.70	0.92 / 0.29
Tiny ImageNet	Tiny ObjectNet	0.51	0.96	0.70	0.68	0.82	0.51	0.79	0.63	0.75 / 0.74
Average		0.63	0.79	0.76	0.60	0.76	0.64	0.76	0.64	0.87 / 0.38

G.2 Results with a smaller test set

Table 6. Experiments with a test set of size 1000, with an equal number of ID and OOD test samples. For RETO and vanilla ensembles, we train 5 ResNet20 models for each setting.

ID data	OOD data	kNN	DPN	Vanilla Ensembles	OE	Mahal.		Mahal-T	MCD	RETO (pretrained)
						AUROC ↑ / FPR@95 ↓				
SVHN	CIFAR10	0.92 / 0.32	1.00 / 0.00	0.97 / 0.12	1.00 / 0.00	0.99 / 0.02	0.99 / 0.05	0.97 / 0.15	1.00 / 0.01	
CIFAR10	SVHN	0.81 / 0.74	0.95 / 0.15	0.92 / 0.22	0.97 / 0.11	0.99 / 0.04	0.99 / 0.04	1.00 / 0.02	1.00 / 0.00	
CIFAR100	SVHN	0.83 / 0.71	0.77 / 0.56	0.84 / 0.52	0.82 / 0.50	0.98 / 0.10	0.98 / 0.08	0.97 / 0.27	0.99 / 0.00	
SVHN[0:4]	SVHN[5:9]	0.54 / 0.92	0.87 / 0.81	0.92 / 0.31	0.85 / 0.48	0.92 / 0.29	0.91 / 0.37	0.91 / 0.49	0.97 / 0.14	
CIFAR10[0:4]	CIFAR10[5:9]	0.59 / 0.86	0.82 / 0.68	0.80 / 0.61	0.82 / 0.59	0.79 / 0.73	0.64 / 0.87	0.69 / 0.75	0.87 / 0.50	
CIFAR100[0:49]	CIFAR100[50:99]	0.51 / 0.96	0.70 / 0.74	0.78 / 0.65	0.74 / 0.69	0.72 / 0.80	0.72 / 0.81	0.70 / 0.74	0.79 / 0.62	
CIFAR10	CIFAR10-C brightness 2	0.54 / 0.93	0.55 / 0.93	0.51 / 0.95	0.52 / 0.94	0.58 / 0.92	0.55 / 0.93	0.52 / 0.94	0.57 / 0.91	
CIFAR10	CIFAR10-C contrast 2	0.94 / 0.20	0.69 / 0.86	0.59 / 0.91	0.62 / 0.89	0.82 / 0.56	0.69 / 0.79	0.82 / 0.91	0.91 / 0.39	
CIFAR10	CIFAR10-C defocus blur 2	0.56 / 0.91	0.48 / 0.95	0.54 / 0.93	0.56 / 0.93	0.67 / 0.81	0.58 / 0.90	0.60 / 0.90	0.80 / 0.66	
CIFAR10	CIFAR10-C elastic 2	0.56 / 0.92	0.47 / 0.97	0.63 / 0.87	0.65 / 0.87	0.71 / 0.76	0.66 / 0.85	0.68 / 0.91	0.84 / 0.62	
CIFAR10	CIFAR10-C fog 2	0.81 / 0.52	0.61 / 0.89	0.53 / 0.93	0.55 / 0.93	0.81 / 0.62	0.71 / 0.73	0.58 / 0.92	0.71 / 0.77	
CIFAR10	CIFAR10-C frost 2	0.50 / 0.92	0.84 / 0.60	0.69 / 0.84	0.69 / 0.85	0.90 / 0.42	0.72 / 0.73	0.59 / 0.95	0.98 / 0.12	
CIFAR10	CIFAR10-C frosted glass blur 2	0.51 / 0.95	0.98 / 0.09	0.89 / 0.42	0.86 / 0.50	0.99 / 0.02	0.99 / 0.04	0.99 / 0.04	1.00 / 0.00	
CIFAR10	CIFAR10-C gaussian noise 2	0.57 / 0.89	0.97 / 0.13	0.83 / 0.62	0.85 / 0.58	1.00 / 0.01	0.99 / 0.02	1.00 / 0.00	1.00 / 0.00	
CIFAR10	CIFAR10-C impulse noise 2	0.61 / 0.85	0.95 / 0.23	0.80 / 0.68	0.81 / 0.61	1.00 / 0.02	0.99 / 0.04	1.00 / 0.00	1.00 / 0.00	
CIFAR10	CIFAR10-C jpeg compression 2	0.51 / 0.95	0.65 / 0.92	0.71 / 0.81	0.73 / 0.77	0.75 / 0.74	0.68 / 0.84	1.00 / 0.00	0.98 / 0.14	
CIFAR10	CIFAR10-C motion blur 2	0.60 / 0.88	0.65 / 0.88	0.71 / 0.81	0.74 / 0.77	0.80 / 0.69	0.79 / 0.61	0.99 / 0.01	0.97 / 0.23	
CIFAR10	CIFAR10-C pixelate 2	0.52 / 0.94	0.82 / 0.67	0.65 / 0.88	0.66 / 0.85	0.79 / 0.71	0.66 / 0.86	0.93 / 0.73	0.96 / 0.25	
CIFAR10	CIFAR10-C shot noise 2	0.53 / 0.92	0.87 / 0.61	0.74 / 0.79	0.75 / 0.82	0.98 / 0.06	0.80 / 0.57	0.96 / 0.23	1.00 / 0.00	
CIFAR10	CIFAR10-C snow 2	0.57 / 0.90	0.85 / 0.61	0.74 / 0.76	0.74 / 0.80	0.96 / 0.18	0.73 / 0.74	0.69 / 0.95	0.99 / 0.11	
CIFAR10	CIFAR10-C zoom blur 2	0.59 / 0.89	0.56 / 0.96	0.71 / 0.77	0.73 / 0.81	0.83 / 0.56	0.77 / 0.66	1.00 / 0.00	0.99 / 0.06	
CIFAR10	CIFAR10-C brightness 5	0.56 / 0.88	0.77 / 0.78	0.60 / 0.90	0.63 / 0.89	0.78 / 0.73	0.79 / 0.72	0.60 / 0.92	0.92 / 0.33	
CIFAR10	CIFAR10-C contrast 5	1.00 / 0.00	0.98 / 0.08	0.92 / 0.25	0.96 / 0.14	1.00 / 0.01	0.99 / 0.04	1.00 / 0.00	1.00 / 0.00	
CIFAR10	CIFAR10-C defocus blur 5	0.65 / 0.82	0.82 / 0.71	0.88 / 0.39	0.92 / 0.25	0.96 / 0.18	0.95 / 0.14	1.00 / 0.00	1.00 / 0.00	
CIFAR10	CIFAR10-C elastic 5	0.59 / 0.89	0.82 / 0.66	0.80 / 0.64	0.78 / 0.74	0.84 / 0.61	0.75 / 0.77	0.92 / 0.55	0.98 / 0.15	
CIFAR10	CIFAR10-C fog 5	0.89 / 0.27	0.93 / 0.32	0.79 / 0.69	0.80 / 0.69	0.98 / 0.10	0.78 / 0.61	1.00 / 0.00	0.99 / 0.02	
CIFAR10	CIFAR10-C frost 5	0.70 / 0.68	0.94 / 0.27	0.84 / 0.59	0.84 / 0.60	0.98 / 0.07	0.79 / 0.61	0.99 / 0.04	1.00 / 0.00	
CIFAR10	CIFAR10-C frosted glass blur 5	0.55 / 0.92	0.97 / 0.11	0.90 / 0.37	0.89 / 0.39	0.99 / 0.05	0.98 / 0.07	1.00 / 0.00	1.00 / 0.00	
CIFAR10	CIFAR10-C gaussian noise 5	0.67 / 0.75	1.00 / 0.01	0.91 / 0.30	0.96 / 0.17	1.00 / 0.00	1.00 / 0.00	1.00 / 0.00	1.00 / 0.00	
CIFAR10	CIFAR10-C impulse noise 5	0.83 / 0.50	0.99 / 0.04	0.94 / 0.17	0.98 / 0.09	1.00 / 0.00	1.00 / 0.00	1.00 / 0.00	1.00 / 0.00	
CIFAR10	CIFAR10-C jpeg compression 5	0.51 / 0.94	0.73 / 0.87	0.79 / 0.68	0.81 / 0.63	0.82 / 0.61	0.68 / 0.88	1.00 / 0.00	1.00 / 0.02	
CIFAR10	CIFAR10-C motion blur 5	0.66 / 0.82	0.81 / 0.71	0.84 / 0.59	0.86 / 0.50	0.91 / 0.27	0.86 / 0.45	1.00 / 0.00	0.99 / 0.03	
CIFAR10	CIFAR10-C pixelate 5	0.56 / 0.92	0.98 / 0.07	0.84 / 0.59	0.88 / 0.49	0.98 / 0.04	0.97 / 0.12	0.99 / 0.07	0.99 / 0.00	
CIFAR10	CIFAR10-C shot noise 5	0.66 / 0.77	0.99 / 0.01	0.91 / 0.30	0.95 / 0.20	1.00 / 0.00	1.00 / 0.01	1.00 / 0.00	1.00 / 0.00	
CIFAR10	CIFAR10-C snow 5	0.61 / 0.84	0.91 / 0.41	0.77 / 0.70	0.79 / 0.72	0.95 / 0.25	0.72 / 0.74	0.82 / 0.80	0.98 / 0.14	
CIFAR10	CIFAR10-C zoom blur 5	0.63 / 0.84	0.72 / 0.90	0.87 / 0.48	0.88 / 0.43	0.96 / 0.12	0.91 / 0.30	1.00 / 0.00	1.00 / 0.00	
CIFAR100	CIFAR100-C brightness 2	0.53 / 0.94	0.54 / 0.93	0.52 / 0.94	0.52 / 0.94	0.55 / 0.93	0.55 / 0.94	0.52 / 0.95	0.55 / 0.93	
CIFAR100	CIFAR100-C contrast 2	0.94 / 0.21	0.62 / 0.87	0.60 / 0.90	0.58 / 0.90	0.75 / 0.71	0.66 / 0.83	0.60 / 0.91	0.73 / 0.83	
CIFAR100	CIFAR100-C defocus blur 2	0.56 / 0.92	0.44 / 0.96	0.55 / 0.92	0.54 / 0.93	0.70 / 0.82	0.69 / 0.80	0.52 / 0.94	0.63 / 0.87	
CIFAR100	CIFAR100-C elastic 2	0.55 / 0.93	0.32 / 0.97	0.61 / 0.88	0.59 / 0.89	0.68 / 0.86	0.66 / 0.85	0.56 / 0.92	0.68 / 0.85	
CIFAR100	CIFAR100-C fog 2	0.82 / 0.52	0.59 / 0.90	0.55 / 0.93	0.53 / 0.93	0.75 / 0.72	0.73 / 0.73	0.54 / 0.93	0.61 / 0.91	
CIFAR100	CIFAR100-C frost 2	0.53 / 0.90	0.73 / 0.76	0.71 / 0.79	0.65 / 0.83	0.82 / 0.65	0.71 / 0.75	0.66 / 0.89	0.94 / 0.50	
CIFAR100	CIFAR100-C frosted glass blur 2	0.50 / 0.95	0.78 / 0.66	0.79 / 0.61	0.72 / 0.72	0.98 / 0.04	0.96 / 0.17	1.00 / 0.00	1.00 / 0.00	
CIFAR100	CIFAR100-C gaussian noise 2	0.56 / 0.89	0.74 / 0.68	0.81 / 0.59	0.79 / 0.56	0.99 / 0.03	0.68 / 0.80	0.99 / 0.01	0.99 / 0.00	
CIFAR100	CIFAR100-C impulse noise 2	0.61 / 0.85	0.83 / 0.59	0.82 / 0.59	0.83 / 0.55	0.99 / 0.03	0.69 / 0.78	0.99 / 0.00	0.99 / 0.00	
CIFAR100	CIFAR100-C jpeg compression 2	0.51 / 0.94	0.63 / 0.86	0.70 / 0.79	0.69 / 0.79	0.71 / 0.82	0.66 / 0.89	0.70 / 0.88	0.88 / 0.61	
CIFAR100	CIFAR100-C motion blur 2	0.60 / 0.89	0.49 / 0.92	0.68 / 0.82	0.63 / 0.85	0.82 / 0.57	0.67 / 0.79	0.68 / 0.89	0.86 / 0.62	
CIFAR100	CIFAR100-C pixelate 2	0.52 / 0.94	0.76 / 0.75	0.63 / 0.88	0.61 / 0.87	0.87 / 0.49	0.57 / 0.91	0.77 / 0.89	0.86 / 0.60	
CIFAR100	CIFAR100-C shot noise 2	0.53 / 0.92	0.70 / 0.77	0.75 / 0.73	0.73 / 0.72	0.94 / 0.23	0.60 / 0.85	0.83 / 0.79	0.98 / 0.11	
CIFAR100	CIFAR100-C snow 2	0.55 / 0.91	0.76 / 0.73	0.73 / 0.77	0.69 / 0.80	0.93 / 0.36	0.61 / 0.88	0.79 / 0.81	0.94 / 0.42	
CIFAR100	CIFAR100-C zoom blur 2	0.59 / 0.90	0.41 / 0.94	0.69 / 0.81	0.63 / 0.85	0.83 / 0.46	0.68 / 0.81	0.71 / 0.90	0.91 / 0.59	
CIFAR100	CIFAR100-C brightness 5	0.53 / 0.93	0.70 / 0.83	0.64 / 0.86	0.62 / 0.87	0.74 / 0.76	0.72 / 0.77	0.60 / 0.90	0.81 / 0.75	
CIFAR100	CIFAR100-C contrast 5	1.00 / 0.01	0.79 / 0.55	0.78 / 0.57	0.82 / 0.53	0.99 / 0.03	0.98 / 0.12	0.99 / 0.00	0.99 / 0.01	
CIFAR100	CIFAR100-C defocus blur 5	0.65 / 0.84	0.54 / 0.83	0.81 / 0.63	0.75 / 0.67	0.96 / 0.15	0.95 / 0.19	0.99 / 0.01	0.99 / 0.03	
CIFAR100	CIFAR100-C elastic 5	0.59 / 0.90	0.73 / 0.78	0.72 / 0.76	0.69 / 0.79	0.71 / 0.81	0.71 / 0.82	0.63 / 0.85	0.89 / 0.57	
CIFAR100	CIFAR100-C fog 5	0.90 / 0.25	0.80 / 0.60	0.75 / 0.70	0.70 / 0.73	0.92 / 0.40	0.80 / 0.67	0.95 / 0.46	0.96 / 0.34	
CIFAR100	CIFAR100-C frost 5	0.73 / 0.68	0.78 / 0.63	0.79 / 0.63	0.72 / 0.71	0.94 / 0.26	0.66 / 0.77	0.95 / 0.45	0.98 / 0.06	
CIFAR100	CIFAR100-C frosted glass blur 5	0.55 / 0.93	0.80 / 0.63	0.80 / 0.60	0.73 / 0.72	0.97 / 0.08	0.76 / 0.70	1.00 / 0.00	1.00 / 0.00	
CIFAR100	CIFAR100-C gaussian noise 5	0.67 / 0.77	0.81 / 0.54	0.84 / 0.42	0.85 / 0.41	1.00 / 0.00	1.00 / 0.00	1.00 / 0.00	1.00 / 0.00	
CIFAR100	CIFAR100-C impulse noise 5	0.84 / 0.48	0.88 / 0.37	0.86 / 0.42	0.96 / 0.20	1.00 / 0.00	1.00 / 0.00	1.00 / 0.00	1.00 / 0.00	
CIFAR100	CIFAR100-C jpeg compression 5	0.51 / 0.94	0.69 / 0.79	0.77 / 0.71	0.75 / 0.69	0.82 / 0.61	0.73 / 0.82	0.94 / 0.50	0.95 / 0.39	
CIFAR100	CIFAR100-C motion blur 5	0.66 / 0.83	0.56 / 0.86	0.76 / 0.70	0.71 / 0.74	0.91 / 0.29	0.77 / 0.64	0.87 / 0.71	0.95 / 0.40	
CIFAR100	CIFAR100-C pixelate 5	0.55 / 0.92	0.95 / 0.17	0.80 / 0.59	0.80 / 0.58	0.99 / 0.01	0.98 / 0.08	0.99 / 0.00	1.00 / 0.00	
CIFAR100	CIFAR100-C shot noise 5	0.66 / 0.79	0.84 / 0.50	0.83 / 0.47	0.84 / 0.44	1.00 / 0.01	1.00 / 0.01	0.99 / 0.00	1.00 / 0.00	
CIFAR100	CIFAR100-C snow 5	0.56 / 0.90	0.80 / 0.63	0.77 / 0.70	0.73 / 0.73	0.90 / 0.45	0.63 / 0.87	0.79 / 0.77	0.96 / 0.37	
CIFAR100	CIFAR100-C zoom blur 5	0.64 / 0.85	0.49 / 0.88	0.79 / 0.66	0.74 / 0.70	0.92 / 0.29	0.93 / 0.24	0.92 / 0.62	0.98 / 0.06	
Average		0.64 / 0.79	0.76 / 0.60	0.76 / 0.64	0.76 / 0.64	0.88 / 0.37	0.79 / 0.53	0.85 / 0.41	0.91 / 0.27	

G.3 Results with VGG

Table 7. Results on all setting where we used ensembles of 5 VGG16 models for RETO and vanilla. For the corruption data sets, we report for each metric the average taken over all corruptions (A), and the value for the worst-case setting (W).

ID data	OOD data	kNN	DPN	Vanilla Ensembles	OE	Mahal.	Mahal-T	MCD	RETO (rand init)	RETO (pretrained)
AUROC ↑ / FPR@95 ↓										
SVHN	CIFAR10	0.92 / 0.32	1.00 / 0.00	0.97 / 0.12	1.00 / 0.00	0.99 / 0.02	0.99 / 0.05	0.97 / 0.15	<u>0.99</u> / <u>0.02</u>	<u>0.99</u> / 0.06
CIFAR10	SVHN	0.81 / 0.74	0.95 / 0.15	0.88 / 0.31	0.97 / 0.11	0.99 / 0.04	0.99 / 0.04	1.00 / 0.02	<u>1.00</u> / <u>0.00</u>	<u>1.00</u> / <u>0.00</u>
SVHN[0:4]	SVHN[5:9]	0.54 / 0.92	0.87 / 0.81	0.89 / 0.40	0.85 / 0.48	0.92 / 0.29	0.91 / 0.37	0.91 / 0.49	<u>0.94</u> / <u>0.34</u>	0.93 / 0.37
CIFAR10[0:4]	CIFAR10[5:9]	0.59 / 0.86	0.82 / 0.68	0.74 / 0.71	0.82 / 0.59	0.79 / 0.73	0.64 / 0.87	0.69 / 0.75	<u>0.95</u> / <u>0.26</u>	0.91 / 0.37
CIFAR10	CIFAR10-C sev 2 (A)	0.59 / 0.84	0.73 / 0.69	0.66 / 0.83	0.70 / 0.80	0.84 / 0.47	0.75 / 0.62	0.82 / 0.50	<u>0.98</u> / <u>0.07</u>	0.94 / 0.21
CIFAR10	CIFAR10-C sev 2 (W)	0.50 / 0.92	0.47 / 0.97	0.51 / 0.95	0.52 / 0.94	0.58 / 0.92	0.55 / 0.93	0.52 / 0.94	<u>0.77</u> / <u>0.67</u>	0.68 / 0.81
CIFAR10	CIFAR10-C sev 5 (A)	0.67 / 0.72	0.89 / 0.40	0.80 / 0.59	0.86 / 0.46	0.94 / 0.20	0.88 / 0.37	0.95 / 0.16	<u>1.00</u> / <u>0.00</u>	0.99 / 0.04
CIFAR10	CIFAR10-C sev 5 (W)	0.51 / 0.94	0.72 / 0.90	0.58 / 0.90	0.63 / 0.89	0.78 / 0.73	0.68 / 0.88	0.60 / 0.92	<u>0.99</u> / <u>0.01</u>	0.95 / 0.28
Average		0.69 / 0.73	0.88 / 0.45	0.82 / 0.49	0.87 / 0.41	0.91 / 0.29	0.86 / 0.39	0.89 / 0.35	<u>0.98</u> / <u>0.11</u>	0.96 / 0.17

G.4 Results with WideResNet

Table 8. Results on all setting where we used ensembles of 5 WRN-28-10 models for RETO and vanilla. For the corruption data sets, we report for each metric the average taken over all corruptions (A), and the value for the worst-case setting (W).

ID data	OOD data	kNN	DPN	Vanilla Ensembles	OE	Mahal.	Mahal-T	MCD	RETO (rand init)	RETO (pretrained)
AUROC ↑ / FPR@95 ↓										
SVHN	CIFAR10	0.92 / 0.32	1.00 / 0.00	0.96 / 0.14	1.00 / 0.00	0.99 / 0.02	0.99 / 0.05	0.97 / 0.15	0.99 / 0.04	<u>1.00</u> / <u>0.01</u>
CIFAR10	SVHN	0.81 / 0.74	0.95 / 0.15	0.94 / 0.19	0.97 / 0.11	0.99 / 0.04	0.99 / 0.04	1.00 / 0.02	<u>1.00</u> / <u>0.00</u>	<u>1.00</u> / <u>0.00</u>
SVHN[0:4]	SVHN[5:9]	0.54 / 0.92	0.87 / 0.81	0.91 / 0.38	0.85 / 0.48	0.92 / 0.29	0.91 / 0.37	0.91 / 0.49	0.94 / 0.29	<u>0.96</u> / <u>0.22</u>
CIFAR10[0:4]	CIFAR10[5:9]	0.59 / 0.86	0.82 / 0.68	0.80 / 0.65	0.82 / 0.59	0.79 / 0.73	0.64 / 0.87	0.69 / 0.75	<u>0.96</u> / <u>0.20</u>	0.94 / 0.29
CIFAR10	CIFAR10-C sev 2 (A)	0.59 / 0.84	0.73 / 0.69	0.69 / 0.82	0.70 / 0.80	0.84 / 0.47	0.75 / 0.62	0.82 / 0.50	<u>0.98</u> / <u>0.08</u>	<u>0.98</u> / 0.10
CIFAR10	CIFAR10-C sev 2 (W)	0.50 / 0.92	0.47 / 0.97	0.51 / 0.95	0.52 / 0.94	0.58 / 0.92	0.55 / 0.93	0.52 / 0.94	<u>0.90</u> / <u>0.43</u>	0.84 / 0.65
CIFAR10	CIFAR10-C sev 5 (A)	0.67 / 0.72	0.89 / 0.40	0.84 / 0.53	0.86 / 0.46	0.94 / 0.20	0.88 / 0.37	0.95 / 0.16	<u>1.00</u> / 0.01	<u>1.00</u> / <u>0.00</u>
CIFAR10	CIFAR10-C sev 5 (W)	0.51 / 0.94	0.72 / 0.90	0.59 / 0.91	0.63 / 0.89	0.78 / 0.73	0.68 / 0.88	0.60 / 0.92	<u>1.00</u> / <u>0.02</u>	0.99 / 0.03
Average		0.69 / 0.73	0.88 / 0.45	0.86 / 0.45	0.87 / 0.41	0.91 / 0.29	0.86 / 0.39	0.89 / 0.35	<u>0.98</u> / <u>0.10</u>	<u>0.98</u> / <u>0.10</u>

G.5 Results on MNIST and FashionMNIST

Table 9. Results on MNIST/FashionMNIST settings. For RETO and vanilla ensembles, we train 5 3-hidden layer MLP models for each setting.

ID data	OOD data	kNN	DPN	Vanilla Ensembles	OE	Mahal.	Mahal-T	MCD	RETO (rand init)	RETO (pretrained)
AUROC ↑ / FPR@95 ↓										
MNIST	FashionMNIST	0.98 / 0.10	1.00 / 0.00	0.81 / 0.99	1.00 / 0.00	1.00 / 0.00	1.00 / 0.00	1.00 / 0.02	<u>1.00</u> / <u>0.00</u>	<u>1.00</u> / <u>0.00</u>
FashionMNIST	MNIST	0.98 / 0.09	1.00 / 0.00	0.87 / 0.58	0.68 / 0.84	0.99 / 0.03	0.99 / 0.04	1.00 / 0.00	<u>1.00</u> / <u>0.00</u>	<u>1.00</u> / <u>0.00</u>
MNIST[0:4]	MNIST[5:9]	0.90 / 0.42	0.99 / 0.03	0.94 / 0.28	0.95 / 0.22	0.99 / 0.02	0.99 / 0.02	0.96 / 0.24	<u>1.00</u> / <u>0.02</u>	0.99 / <u>0.02</u>
FashionMNIST[0,2,3,7,8]	FashionMNIST[1,4,5,6,9]	0.74 / 0.67	0.77 / 0.85	0.64 / 0.93	0.66 / 0.88	0.77 / 0.80	0.82 / 0.61	0.78 / 0.70	<u>0.95</u> / <u>0.27</u>	0.93 / 0.38
Average		0.90 / 0.32	0.94 / 0.22	0.82 / 0.70	0.82 / 0.49	0.94 / 0.21	0.95 / 0.17	0.94 / 0.24	<u>0.99</u> / <u>0.07</u>	0.98 / 0.10

For FashionMNIST we chose this particular split (i.e. classes 0,2,3,7,8 vs classes 1,4,5,6,9) because the two partitions are more similar to each other. This makes OOD detection more difficult than the 0-4 vs 5-9 split.

G.6 More results for Outlier Exposure

Table 10. Results for Outlier Exposure, when using the same corruption type, but with a higher/lower severity, as OOD data seen during training.

ID data	OOD data	OE (trained on sev5)	OE (trained on sev2)
		AUROC \uparrow	
CIFAR10	CIFAR10-C sev 2 (A)	0.89	N/A
CIFAR10	CIFAR10-C sev 2 (W)	0.65	N/A
CIFAR10	CIFAR10-C sev 5 (A)	N/A	0.98
CIFAR10	CIFAR10-C sev 5 (W)	N/A	0.78
CIFAR100	CIFAR100-C sev 2 (A)	0.85	N/A
CIFAR100	CIFAR100-C sev 2 (W)	0.59	N/A
CIFAR100	CIFAR100-C sev 5 (A)	N/A	0.97
CIFAR100	CIFAR100-C sev 5 (W)	N/A	0.67
Average		0.87	0.98

The Outlier Exposure method needs access to a set of OOD samples during training. The numbers we report in the rest of paper for Outlier Exposure are obtained by using the TinyImages data set as the OOD samples that are seen during training. In this section we explore the use of an $\text{OOD}_{\text{train}}$ data set that is more similar to the OOD data observed at test time. This is a much easier setting for the Outlier Exposure method: the closer $\text{OOD}_{\text{train}}$ is to OOD_{test} , the easier it will be for the model tuned on $\text{OOD}_{\text{train}}$ to detect the test OOD samples.

In the table below we focus only on the settings with corruptions. For each corruption type, we use the lower severity corruption as $\text{OOD}_{\text{train}}$ and evaluate on the higher severity data and vice versa. We report for each metric the average taken over all corruptions (A), and the value for the worst-case setting (W).

H Experiments on CIFAR10v2

Here we will present our results on distinguishing between CIFAR10 [22] and CIFAR10v2 [36], a data set meant to be drawn from the same distribution as CIFAR10 (generated from the Tiny Images collection [44]). In the paper [37], the authors argue that CIFAR10 and CIFAR10v2 come from very similar distributions. They provide supporting evidence by training a binary classifier to distinguish between them, and observing that the accuracy that is obtained of 52.9% is very close to random.

Our experiments show that the two data sets are actually distinguishable, contrary to what previous work has argued. First, our own binary classifier trained on CIFAR10 vs CIFAR10v2 obtains a test accuracy of 67%, without any hyperparameter tuning. The model we use is a ResNet20 trained for 200 epochs using SGD with momentum 0.9. The learning rate is decayed by 0.2 at epochs 90, 140, 160 and 180. We use 1600 examples from each data set for training, and we validate using 400 examples from each data set.

Table 11: OOD detection performance on CIFAR10 vs CIFAR10v2

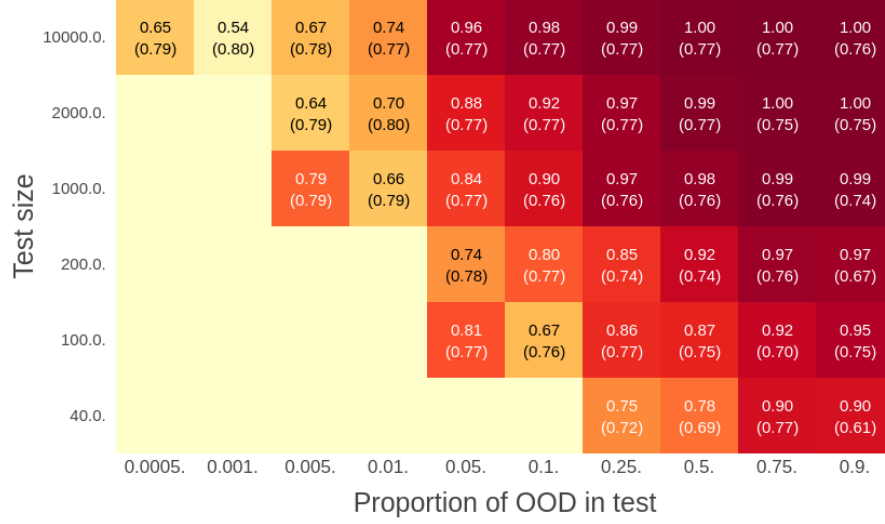
ID data	OOD data	kNN	DPN	Vanilla Ensembles	OE	Mahal. AUROC \uparrow / FPR@95 \downarrow	Mahal-T	MCD	RETO (rand init)	RETO (pretrained)
CIFAR10	CIFAR10v2	0.53 / 0.93	0.63 / 0.91	0.64 / 0.87	0.64 / 0.88	0.55 / 0.92	0.56 / 0.93	0.58 / 0.90	0.91 / 0.20	0.76 / 0.74

Furthermore, our OOD detection experiments (presented in Table 11) show that most baselines are able to distinguish between the two data sets, with RETO achieving the highest performance. The methods which require OOD data for tuning (Outlier Exposure and DPN) use CIFAR100.

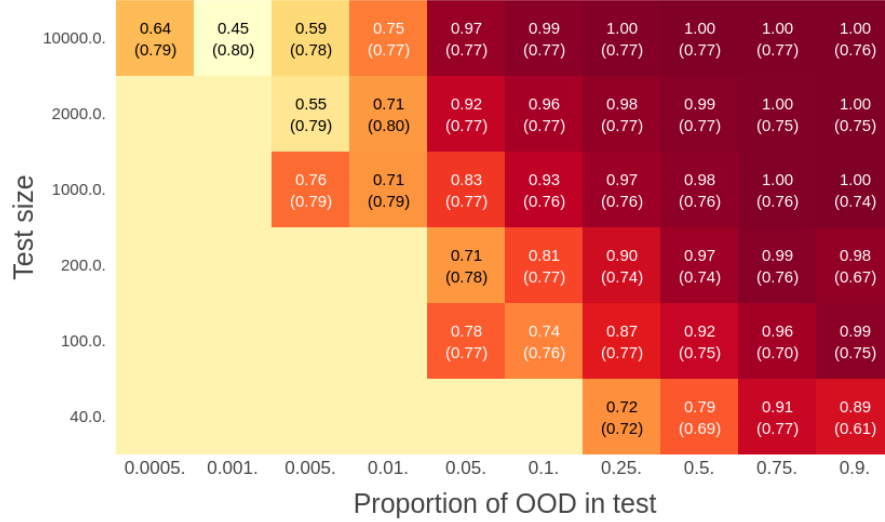
I Dependence on the test set configuration

In order to bridge the gap between (offline) transductive OOD detection and online anomaly detection we investigate the impact of the size of the test set on the OOD detection performance. In addition, we also vary the ratio of OOD samples in the test set, i.e. $\frac{|T_{\text{OOD}}|}{|T_{\text{ID}}|+|T_{\text{OOD}}|}$. Our findings suggest that there is a broad spectrum of values for which RETO maintains a good performance. In Figures 11a and 11b we show the AUROC of RETO and vanilla ensembles for various configurations of the test set, when the RETO method is trained from pre-trained weights or random initializations. For RETO, we use a smaller batch size of 32. The reason is that, for settings where there is almost no OOD data, larger batch sizes (like 128) will ‘drown out’ the signal from OOD samples, since there will be so few of them per batch, compared to the ID samples.

However, when there are only a few very diverse OOD test samples, their contribution to the gradient is small. Moreover, if the number of ID test samples is large, fitting a single arbitrary label on them is much easier. As a consequence, the arbitrary label can take longer to fit on the (few) OOD samples, than on the (many) test ID samples, leading to false positives, i.e. ID samples incorrectly flagged as OOD. This loss in efficacy can be mitigated by either splitting the test set in smaller batches, or by using a different labeling scheme for the test set, the details of which we leave as future work. Alternatively, one can use both an inductive and a transductive method to do OOD detection: the transductive method ensures high detection accuracy, if there are enough OOD samples in the test batch, while the inductive method can be used as a fallback solution.



(a) Initialization from pre-trained weights.



(b) Initialization from random weights.

Figure 11. AUROCs obtained with an ensemble of ResNet20 models as the composition of the test set is changed. Only settings with at least 5 OOD samples have been considered. The ID samples are from CIFAR10, while the OOD samples are from CIFAR10-C/snow5. For comparison, we provide in parentheses AUROC values for a vanilla ensemble trained once on the training set and evaluated on each test set configuration. (a) The models are initialized from pre-trained weights. (b) The models are initialized with random weights.

J Effect of learning rate and batch size

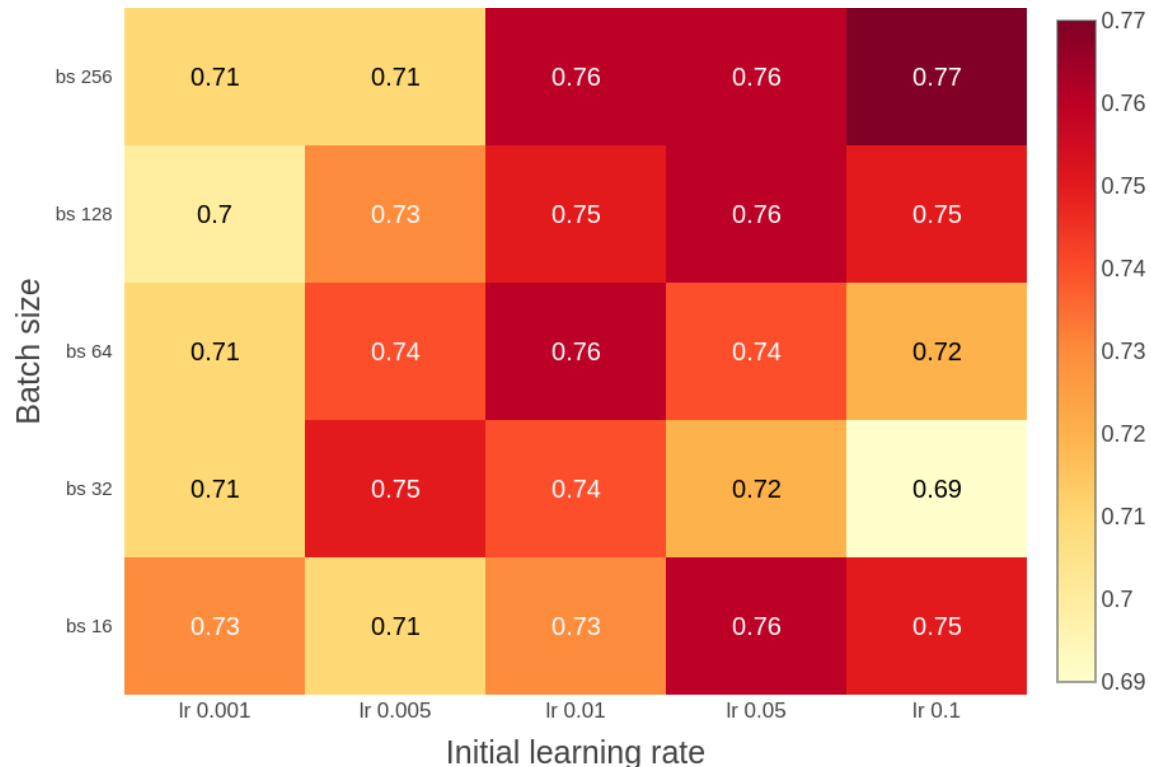


Figure 12. AUROCs obtained with an ensemble of WRN-28-10 models, as the initial learning rate and the training batch size are varied. For this we used the hardest setting, CIFAR100:0-50 as ID, and CIFAR100:50-100 as OOD.

K Medical OOD detection benchmark

The medical OOD detection benchmark is organized as follows. There are four training (ID) data sets, from three different domains: two data sets with chest X-rays, one with fundus imaging and one with histology images. For each ID data set, the authors consider three different OOD scenarios:

1. Use case 1: The OOD data set contains images from a completely different domain, similar to our category of easy OOD detection settings.
2. Use case 2: The OOD data set contains images with various corruptions, similar to our category of hard covariate shift settings.
3. Use case 3: The OOD data set contains images that come from novel classes, not seen during training.

The authors evaluate a number of methods on all these scenarios. The methods can be roughly categorized as follows:

1. Data-only methods: Fully non-parametric approaches like kNN.
2. Classifier-only methods: Methods that use a classifier trained on the training set, e.g. ODIN [28], Mahalanobis [26]. RETO falls into this category as well.
3. Methods with Auxiliary Models: Methods that use an autoencoder or a generative model, like a Variational Autoencoder or a Generative Adversarial Network. Some of these approaches can be expensive to train and difficult to optimize and tune.

We stress the fact that for most of these methods the authors use (known) OOD data during training. Oftentimes the OOD samples observed during training come from a data set that is very similar to the OOD data used for evaluation.

For exact details regarding the data sets and the methods used for the benchmark, we refer the reader to the paper [8].

We did not evaluate RETO on the histology image data set due to resource limitations; the data set is much larger than the others.

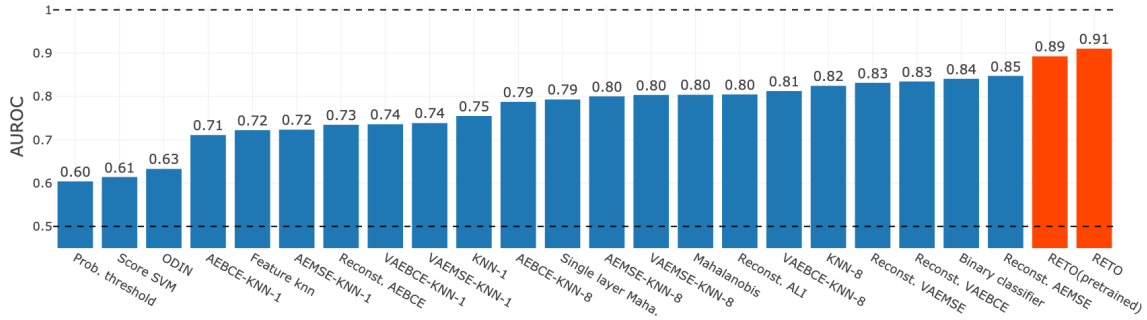


Figure 13. AUROC averaged over all scenarios in the medical OOD detection benchmark [8]. The values for all the baselines are computed using code made available by the authors of the paper [8]. Notably, most of the baselines assume oracle knowledge of OOD data at training time.

In Figures 14, 15, 16 we present AUROC and AUPR (Area under the Precision Recall curve) for RETO for each of the training data sets, and each of the use cases. Figure 13 presents averages over all settings that we considered, for all the baseline methods in the benchmark. Notably, RETO performs well consistently across data sets.

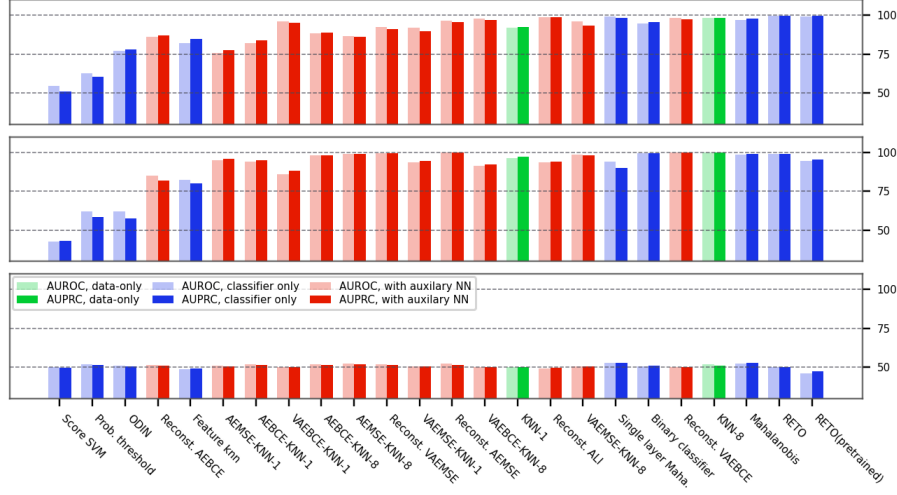


Figure 14. Comparison between RETO and the various baselines on the NIH chest X-ray data set, for use case 1 (top), use case 2 (middle) and use case 3 (bottom).

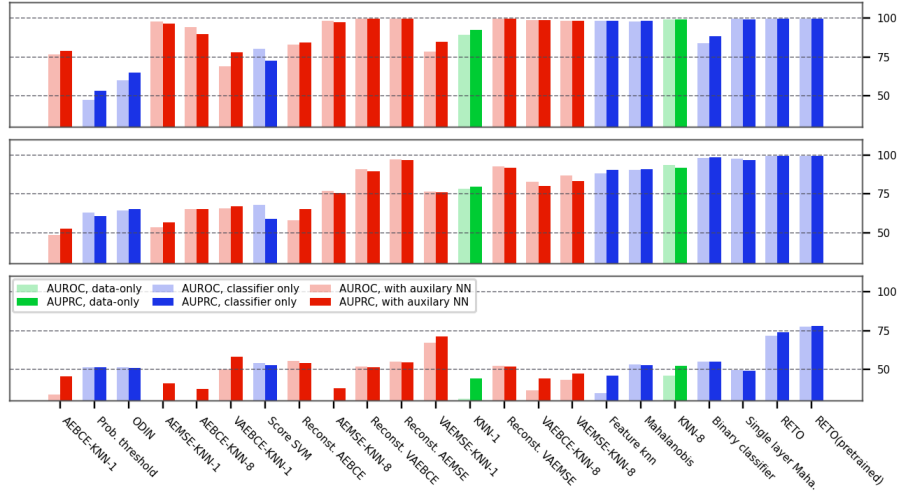


Figure 15. Comparison between RETO and the various baselines on the PC chest X-ray data set, for use case 1 (top), use case 2 (middle) and use case 3 (bottom).

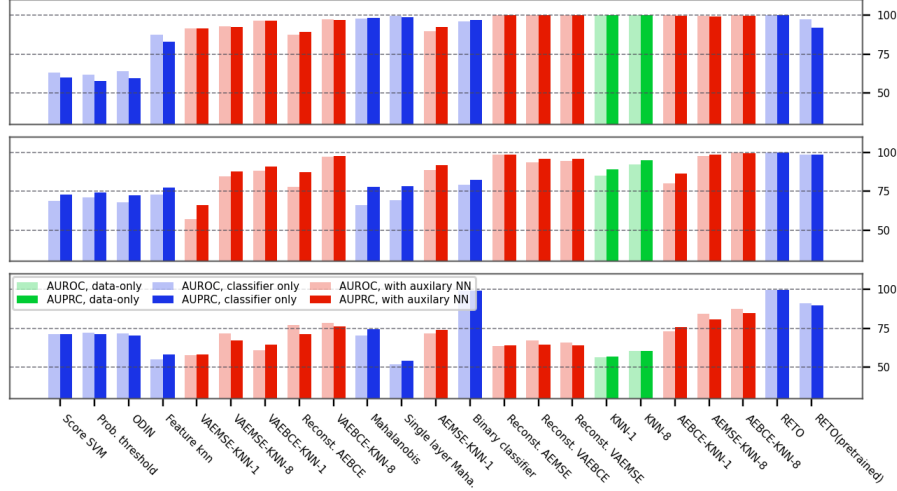


Figure 16. Comparison between RETO and the various baselines on the DRD fundus imaging data set, for use case 1 (top), use case 2 (middle) and use case 3 (bottom).

For all of medical benchmarks, we have kept the test set balanced, with an equal number of ID and OOD samples (subsampling the bigger dataset, if necessary).

L Hypothesis test for OOD detection

We distinguish between ID and OOD data using an approach reminiscent of a two-sample statistical test. Consider two finite-sample sets, namely the training set $\{x_i : x_i \sim P_X, 1 \leq i \leq n\}$ and the set that only contains one test point $\{x : x \sim Q_X\}$. We are interested in identifying anomalous covariates, so we discard the labels when performing the statistical test. The null hypothesis is $H_0 : \text{supp}_P = \text{supp}_Q$ and, if it is rejected, it indicates that the test sample x is OOD. The various OOD detection methods differ in their choice of the test statistic. For approaches that use ensembles of classifiers, the test statistic should reflect the belief that the models have similar outputs on ID samples, and disagree on OOD samples. For example, the paper [24] proposes averaging the softmax outputs of all the models in the ensemble and then taking the maximum or the entropy of the resulting probability vector as the test statistic. For a K -model ensemble and an input x this can be written as follows:

$$T_{\text{max-p}}(x) := \max_{i \in \mathcal{Y}} \frac{1}{K} \sum_{k=1}^K (f_k(x))_i, \text{ with } f_k(x) \in \mathbb{R}^{|\mathcal{Y}|} \text{ the softmax output of the } k^{\text{th}} \text{ model.}$$

Averaging the softmax vectors loses some information about the model predictions, because different initial probability vectors can map to the same averaged vector. In our approach, models are more uncertain on ID samples than on OOD samples, which can make the averaged softmax vector fall at the same location for an ID and an OOD sample. This makes it impossible to distinguish between the two, as illustrated in Figure 17.

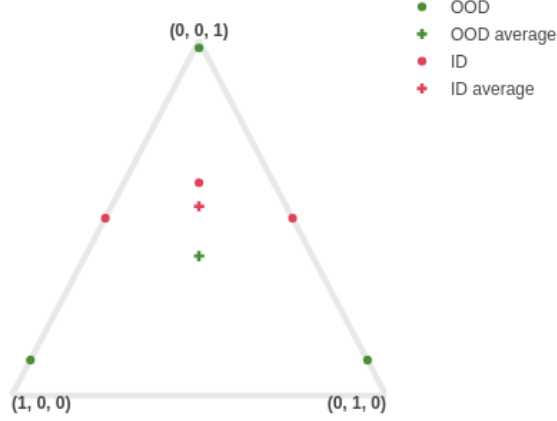


Figure 17. Averaging the probability outputs of the models in an ensemble can lead to catastrophic information loss, in some cases. The softmax vectors of a 3-model ensemble are represented on the 2D probability simplex. For an OOD sample, each model predicts with high confidence the arbitrary label it has seen during training. For the ID sample, the models predict the correct class with moderate confidence. Therefore, the average probability vectors for the ID and the OOD sample are close, which can make it hard to distinguish between them.

For neural network ensembles, following a standard training procedure of minimizing the cross-entropy loss leads to models that make confident predictions on both ID and OOD samples, as shown by [18, 30]. Consequently, the information lost through averaging is not causing any issues: on ID samples, the models will tend to give the same prediction, while on OOD samples the models tend to disagree, giving different predictions with high confidence in both cases.

However, in our situation, because of early stopping, the training process is halted at different stages for test ID and test OOD samples, as indicated in Figure 5.

Recent papers like [42, 9] analyze the dynamics of optimizing the cross-entropy loss with SGD. They suggest that there might exist two stages: one in which a good decision boundary is found, and another in which the margin is increased between the representations of inputs from different classes. It is this second stage that also leads to overconfident predictions on both ID and OOD samples. Thus, early stopping may cause the models to be more uncertain on test ID samples than on test OOD. This is indeed shown in Figure 18.

To avoid the problem of information loss described previously, we compute the pairwise total variation distances between the softmax outputs of the models in the ensemble, and we take the average of these distances as our test statistic:

$$T_{\text{avg-TV}}(x) := \frac{2}{K(K-1)} \sum_{\substack{i,j=1 \\ i < j}}^K d_{\text{TV}}(f_i(x), f_j(x))$$



Figure 18. Distribution of confidence for a model trained on the ID training set alone (**Top**) and a model trained on both the training set and the arbitrarily labeled test set (with both ID and OOD samples), with early stopping (**Middle**) and after 100 epochs (**Bottom**). The models in the vanilla ensemble are confident on both ID and OOD samples. The early-stopped model trained on training+test is confident only on the OOD data, even though at convergence it has a high confidence on the test ID samples as well.